

RESEARCH

Open Access



# Copper's new role in cancer: how cuproptosis-related genes could revolutionize glioma treatment

Yu Wang<sup>1†</sup>, Sen Qiao<sup>3†</sup>, Ping Wang<sup>1†</sup>, Mi Li<sup>2</sup>, Xiaozhen Ma<sup>2</sup>, Hongmei Wang<sup>2\*</sup>  and Junhong Dong<sup>1\*</sup>

## Abstract

**Objectives** Cuproptosis, a novel form of regulatory cell death, was investigated in this study for its effects on cuproptosis-associated proteins during gliomas development, offering novel insights into the mechanism of copper ion-based antitumor drugs.

**Methods** In the present study, bioinformatics and cellular experiments were employed to investigate cuproptosis-related genes (CRGs) in glioma, with a specific focus on SLC31A1.

**Results** The study findings indicated that many CRGs (SLC31A1, FDX1, DLST, LIPT1, LIPT2, DLD, NFE2L2, ATP7A, DLAT, GCSH, and ATP7B) were differentially expressed between glioma and non-tumor groups. These genes potentially influence glioma initiation and progression by modulating associated signaling pathways, including those involved in cell cycle regulation, inflammatory responses, and the tumor microenvironment. Survival curve analysis and Cox proportional hazard regression model demonstrated that individuals classified as high-risk exhibited poorer prognosis, suggesting that CRGs possess prognostic capabilities. The assessment of tumor mutational burden indicated that CRGs could serve as biomarkers for predicting the efficacy of immunotherapy in glioma. Further functional analysis of SLC31A1 showed that its elevation was associated with increased glioma cell malignancy, promoting proliferation and migration. Additionally, treatment with the mitotic inhibitor MP-HJ-1b markedly suppressed SLC31A1 expression, consequently inhibiting glioma cell proliferation and migration.

**Conclusions** Extensive data analysis indicated that CRGs hold promise as both prognostic markers and potential therapeutic targets for glioma.

**Keywords** Glioma, Cuproptosis-related genes, Prognosis, SLC31A1, Immune infiltration, MP-HJ-1b

<sup>†</sup>Yu Wang, Sen Qiao and Ping Wang contributed equally to this work.

\*Correspondence:

Hongmei Wang  
wanghongmei@sntcm.edu.cn  
Junhong Dong  
djh196@163.com

<sup>1</sup>School of Basic Medical Sciences, Shandong Second Medical University, NO. 7166 Baotong West Street, Weifang 261053, China

<sup>2</sup>School of Basic Medicine, Shaanxi University of Chinese Medicine, No.1, Middle Century Avenue, Chenyangzhai, Xianyang 712046, Shaanxi, China

<sup>3</sup>Assisted Reproduction Center, Northwest Women's and Children's Hospital, No.73 Houzaimen, North Street, Xincheng District, Xi'an 710003, China



## Introduction

Based on the 2020 global cancer statistics, 251,329 deaths were attributed to primary central nervous system cancers, accounting for 2.5% of all cancer-related deaths [1]. Notably, gliomas, particularly glioblastoma (GBM) and diffuse low-grade gliomas, represent approximately 80% of all malignant brain tumors in adults and pose a significant threat to human health [2]. At present, the primary treatment approach involves extensive resection, complemented by chemotherapy (with temozolomide [TMZ] as the standard medication) or radiotherapy. Due to the intricate anatomical structure and functional complexity of the central nervous system, as well as the invasive nature of glioma cells, achieving complete resection remains challenging. Additionally, the presence of blood–brain barrier limitations, radiotherapy resistance, and chemotherapy resistance significantly hinder the prognosis of glioma treatment, leading to high postoperative recurrence and poor long-term patient survival [3–5]. However, complete resection remains challenging due to the complex anatomical architecture and functional intricacy of the central nervous system, along with the infiltrative nature of glioma cells.

Copper ions, an essential metal with redox properties, act as cofactors for various enzymes that participate in critical biological processes, including mitochondrial respiration, free radical scavenging, iron uptake, tyrosine metabolism, and melanin synthesis [6]. Indeed, maintaining copper homeostasis throughout the body is critical for optimal cellular metabolic function, as excessive copper ion accumulation can cause copper toxicity and subsequent cell death. Cuproptosis, a distinct form of regulated cell death, distinct from other cell death-mechanisms, such as apoptosis, ferroptosis, pyroptosis, and necroptosis [7]. Copper homeostasis has been implicated in a wide range of diseases, such as tumors, ischemic heart disease, Alzheimer's disease, and renal fibrosis [8–10]. As a cofactor for mitochondrial cytochrome c oxidase (COX), copper is essential for meeting the energy requirements of rapidly proliferating cells. Consequently, serum copper ion concentrations are elevated in patients with various malignancies, including leukemia, lung cancer, thyroid cancer, gallbladder cancer, colorectal cancer, prostate cancer, breast cancer, and pancreatic cancer, reflecting the increased demand for copper [11–13].

Research has demonstrated that copper homeostasis is associated with tumor development and progression. Copper can bind to PDK1 in a manner dependent on the copper transporter 1 (CTR1, also known as SLC31A1), thereby activating AKT kinase and influencing tumor formation by modulating the PI3K-PDK1-AKT signal transduction [14]. A related study found that the malignant biological behaviors of gliomas, including proliferation, growth, and colony-forming ability, were inhibited

following siRNA-mediated RARRES2 (a type of CRGs) knockdown in glioma cell lines [15]. Caroline et al. down-regulated copper homeostasis in hepatocellular carcinoma cell lines by combining SLC31A1 knockdown and tetrathiomolybdate (TTM, a copper-specific chelator) treatment, which disrupted copper availability and inhibited proliferative growth and colony formation [16].

Copper ions may augment the proliferation and migration of two distinct cancer cell lines (A549 and DU145) by amplifying the RTK signaling pathway [17]. The study findings indicate that the administration of siSLC31A1 significantly impairs survival and reduces the migratory potential of pancreatic cancer cells, likely due to decreased intracellular copper availability [18]. Notably, related studies have indicated that copper homeostasis is closely linked to epithelial–mesenchymal transition (EMT) in tumors [19]. Another study demonstrated that treatment with the copper chelator triethylenetetramine induced EMT and altered migratory ability in breast cancer cell lines, with these effects varying among different breast cancer subtypes. Further research revealed that this phenomenon may be linked to the effects of copper depletion on the AKT/GSK3 $\beta$ /SNAIL and TGF $\beta$ /STAT3 axes [20]. Onuma et al. suggested that copper-induced differentially expressed genes play a role in facilitating angiogenesis in both ovarian cancer and mesothelioma cells. Of note, increased copper concentration increased vascular endothelial growth factor (VEGF) mRNA levels within ovarian cancer cell lines [21]. It has been substantiated that copper plays a pivotal role in the regulation of angiogenesis [22, 23]; consequently, this phenomenon significantly impacts the nutritional status, proliferation rate, and migratory behavior of tumor cells.

The regulatory mechanisms underlying copper-induced cell death are intricately linked to mitochondrial metabolism. Specifically, surplus copper directly interacts with lipoacylated proteins in the mitochondrial TCA cycle, thereby inducing the anomalous aggregation of lipoacylated proteins and depletion of iron–sulfur cluster-containing proteins within the respiratory chain complex. These events result in a protein-toxic stress response, ultimately leading to cell death. Given the research context and significance of copper-induced cell death, we investigated specific genes associated with this phenomenon to elucidate their role in glioma.

## Materials and methods

### Ualcan

UALCAN (<https://ualcan.path.uab.edu/index.html>), an online platform, facilitates the extraction and examination of diverse cancer histology datasets, encompassing The Cancer Genome Atlas (TCGA), MET500, and CPTAC. The present research utilized the gene expression analysis features provided by UALCAN to

investigate the contrasting expression patterns of CRGs in glioma as compared to normal tissues. In our study, the levels of CRGs were obtained through the “Expression” links, utilizing the “TCGA analysis” module in conjunction with the glioma dataset.

#### **GEPIA**

The GEPIA database (<http://gepia.cancer-pku.cn/>), incorporating sequencing data from 9736 cancerous and 8587 normal paracancerous tissues derived from the GTEx and TCGA databases, facilitates the execution of expression, survival, and downstream analyses. In this study, GEPIA was utilized to investigate the potential association between CRGs and the pathological stage of glioma and to assess the expression patterns of CRGs in glioma. Specifically, we conducted a pathological stage analysis and a multiple gene comparison analysis of CRGs. Additionally, the correlation between CRGs and disease-free survival (DFS) was analyzed. We opted for the “stage plots” available on the aforementioned website, using the overall survival (OS) dataset for the analysis of differential expression of CRGs across various pathological stages.

#### **Kaplan–meier plotter**

The Kaplan-Meier Plotter (<https://kmplot.com/analysis/>), a comprehensive database incorporating correlations between gene expression and prognostic significance in 3,000 samples across 21 unique cancer types, provides researchers the ability to perform survival analyses on specific genes of interest. For this study, the database was employed to examine the correlation between OS and recurrence-free survival (RFS) with CRGs in glioma. The Kaplan-Meier Plotter (<https://kmplot.com/analysis/>) is equipped to evaluate the impact of 54k genes (mRNA, miRNA, and protein) on survival across 21 cancer types, including GBM multiforme ( $n=153$ ) and low-grade glioma ( $n=513$ ). The data sources for these databases comprise GEO, EGA, and TCGA. For this study, the glioma database on the aforementioned website was selected, the candidate genes were input, and OS (RFS) was chosen to execute survival analysis. A  $p$ -value less than 0.05 was considered statistically significant. The relationship between CRGs and survival in glioma patients was assessed using Kaplan-Meier curves and tested using the log-rank test. Risk ratios (HR) for CRGs expression in gliomas determined using univariate and multivariate Cox regression, Lasso regression was used for variable optimization to avoid overfitting.

#### **cBioPortal**

The cBioPortal website (<https://www.cbioportal.org/>) functions as a comprehensive platform for collating data obtained from 126 tumor genomic studies conducted

within the TCGA and ICGC large-scale oncology research initiatives, which include 28,000 unique specimens. This valuable resource facilitates the visual scrutiny of multifaceted cancer genomic data, particularly enabling the investigation of mutations within CRGs among patients in glioma patients. On this website, we chose the glioma dataset to study the genetic alterations of the CRGs.

#### **GeneMANIA**

GeneMANIA (<http://genemania.org/>) is a comprehensive database that is used to generate hypotheses regarding gene function as well as analyze gene lists and prioritization based on their functional attributes. In this study, GeneMANIA was employed to investigate the interaction of neighboring genes with CRGs.

#### **Bioinformatics**

Bioinformatics functions (<http://www.bioinformatics.com.cn/>) as a potent online platform for conducting bioinformatic analyses, enabling the effective processing and visualization of various research data. The DAVID bioinformatic resources (<https://david.ncifcrf.gov>), comprising an integrated biological knowledgebase and analytic tools, allow for the systematic extraction of biological significance from extensive gene/protein lists. In the context of this study, this tool was employed to proficiently inspect and visualize the Gene Ontology (GO) and Kyoto Encyclopedia of Genes and Genomes (KEGG) pathways linked with CRGs. The functional enrichment analyses were executed using the R package ClusterProfiler (version: 3.18.0).

#### **Timer**

Utilizing TCGA database (<https://www.cancer.gov/about-nci/organization/ccg/research/structural-genomics/tcga>), we examined the correlation between CRGs and glioma, and determined the relationship between CRGs and immune cell infiltration. The Timer online analysis tool (<http://timer.cistrome.org/>) uses RNA-seq expression profiling data to detect immune cell infiltration in various tumor tissues and assess its impact on clinical prognosis. This database was employed to investigate the correlation between CRGs and immune cell infiltration, as well as their respective influences on prognosis.

#### **LN229 cell culture**

The LN229 cell line was obtained from the American Type Culture Collection (ATCC), and the cell line quality met the essential criteria for the cellular experiments cultured in this study. LN229 cells were nurtured in high-glucose Dulbecco’s Modified Eagle Medium (DMEM, Thermo Fisher Scientific Inc., MA, USA) supplemented with 10% fetal bovine serum (FBS, Thermo Fisher

Scientific Inc.) and 1% penicillin-streptomycin. The cells were incubated at 37 °C in an humidified atmosphere containing 5% CO<sub>2</sub>.

#### Establishment of stable cell lines

The LN229 cells were treated using two methods, RNA interference-mediated knockdown and overexpression, targeting the gene SLC31A1 (NM\_001859). The interference RNA sequence for SLC31A1 was designed by Shandong Weizhen Biotechnology Co., Ltd. Three interference sequences were designed based on the cDNA sequence provided by GenBank. Following preliminary experiments, the sequence with the highest interference efficiency was selected: sh-SLC31A1: GCAACAGATGCTGAGCTTTCCTTCAAGAGAGGAAAGCTCAGCATCTGTTGCTTTTTT. The negative control sequence is: TTCTCCGAACGTGTCACGTTTCAAGAGAACGTGACACGTTTCGGAGAATTTTTT. Total RNA was extracted from LN229 cells, and the target sequence containing BamHI and EcoRI (Takara Biotechnology Co., Ltd., Beijing, China) restriction sites was obtained through PCR and double enzyme digestion. The shRNA-SLC31A1 sequence (shRNA-SLC31A1 group) and its negative control sequence (shRNA-Con group), the target sequence containing BamHI and EcoRI restriction sites (Overexpression-SLC31A1 group) and its negative control sequence (Vector group) were ligated to the plasmid vector to construct recombinant plasmids. These recombinant plasmids were transfected into HEK293T cells, and the supernatant was collected for infecting LN229 cells (cell density was 40%) after stable transfection. Stable cell lines expressing shRNA-SLC31A1, shRNA-Con, Overexpression-SLC31A1, and Vector were obtained and passaged 3–4 times before being stored in liquid nitrogen.

#### RNA extraction and quantitative Real-Time polymerase chain reaction (qRT-PCR)

The Trizol method was selected for the extraction of total cellular RNA. Following cell washing and digestion, the cells were centrifuged at 1000 rpm for 5 min at room temperature. The supernatant was then discarded, and the cells were collected and subsequently treated with Trizol reagent (Qiagen, Hilden, Germany) for cell lysis. Post-extraction, the purity and concentration of RNA were assessed, and the RNA was stored at -80 °C for future use. For qRT-PCR of RNA, the reverse transcription and qRT-PCR systems was established using the PrimeScript™ RT (Takara Biotechnology Co., Ltd.) premix and SYBR Premix Ex Taq™ II (Takara Biotechnology Co., Ltd.) reagent kit. The reference gene utilized was GAPDH, and the calculation method employed was  $2^{-\Delta\Delta C_t}$ . qRT-PCR was conducted to validate the expression levels of SLC31A1 in different cell groups. The primer sequences for real-time fluorescent quantitative PCR were as follows:

#### SLC31A1

Forward: 5'-ATGGAACCATCCTTATGGAGACA-3'  
Reverse: 5'-GGAAGTAGCTTATGACCACCTGG-3'

#### GAPDH

Forward: 5'-TGACTTCAACAGCGACACCCA-3'  
Reverse: 5'-CACCTGTGTGCTGTAGCCAAA-3'

The experiment was replicated three times, and the average of the experimental outcomes was considered the final result.

#### Western blot analysis

Proteins were extracted by using the RIPA buffer (Beijing Solarbio Science & Technology Co., Ltd., Beijing, China) from the cells in each group for processing. A 10% separating gel and a 5% stacking gel were prepared. 5 μg of sample and 2 μL of marker were added. Electrophoresis was performed under the following conditions: 10 V for 10 min, 80 V for 30 min, and 120 V for 90 min. The proteins were transferred from the gel to a PVDF membrane. Post-transfer, the membrane was blocked with 5% skim milk powder shaken at room temperature for 1 h. The membrane was washed three times with TBST buffer by shaking. Subsequently, the membranes were incubated with primary antibodies, including SLC31A1 (1:1000, Proteintech Group, Inc, Wuhan, China, RGAM004), and β-actin (1:1000, Proteintech Group, Inc, 20536-1-AP) at 4 °C overnight. The following day, the membrane was washed three times with TBST buffer by shaking. The membrane was then incubated with the secondary antibody (1:5000, Proteintech Group, Inc, SLC31A1:SA00001-2, β-Actin: SA00001-1) at room temperature for 1 h. After three washes with TBST buffer, the developing solution was added, and protein bands were visualized using enhanced chemiluminescence (ECL, Shanghai Epizyme Biomedical Technology Co., Ltd, Shanghai, China) substrate under dark conditions, image acquisition was performed by (Shanghai Tanon Life Science Co., Ltd., Shanghai, China) and photography analysis by ImagJ (Java 1.5.0\_09). The experiment was repeated three times, and the average of the experimental results was calculated as the final result.

#### CCK-8 proliferation assay

The number of cells in each group to be processed was counted. In a 96-well plate,  $1.5 \times 10^3$  cells were inoculated per well. If the volume was less than 100 μL, supplementation with complete culture medium was performed. The cells were cultivated in a humidified CO<sub>2</sub> incubator at 37 °C. Cell proliferation was detected on the 1st, 2nd, 3rd, 4th, and 5th day after cell inoculation. Following the instructions of the CCK-8 kit (Biosharp, BS350A, Beijing Solarbio Science & Technology Co., Ltd., Beijing, China), 10 μL of CCK-8 reagent was added to each well and

incubated at 37 °C for 2 h. After the incubation period, the absorbance of each well was measured using an automatic enzyme-linked immunosorbent assay reader (Thermo Fisher Scientific, USA), with a wavelength set at 450 nm. The experiment was repeated 3 times, and the average of the experimental results was taken as the final result.

#### **Transwell experiment**

The cells in each group to be processed should be counted first. Subsequently, inoculate  $4 \times 10^4$  cells into small chambers contain with 0.33 mg/ml of Matrigel (Corning, Inc., MA, USA), with each chamber receiving 300  $\mu$ l of serum-free medium. Place the chambers in a 24-well plate with 1% penicillin-streptomycin and 10% FBS complete medium, adding 500  $\mu$ l of complete medium to each well. The plates were incubated in a humidified CO<sub>2</sub> incubator at 37 °C with a 5% CO<sub>2</sub> concentration for 24 h. Following this, fix and stain the cells with 4% paraformaldehyde and 0.5% crystal violet, then capture images under a microscope and analyze them using ImageJ software. Repeat the experiment thrice and calculate the average of the results obtained as the final outcome.

#### **Cell scratch assay**

The cell count in each experimental group was determined. A total of  $4 \times 10^5$  cells were inoculated per well in a 6-well plate. The cells were cultured in a humidified CO<sub>2</sub> incubator at 37 °C with a CO<sub>2</sub> concentration of 5%. Once the cells adhered to the bottom of the culture dish, a sterile 10  $\mu$ l pipette tip was used to create a horizontal scratch across the bottom of the dish. The dish was then washed three times with PBS, and DMEM basic culture medium was added for further cultivation. Microscope images were captured at 0 and 24 h post-scratch. The healing rate of the scratch in different groups was calculated by comparing the scratch area in the images before and after. The experiment was repeated three times and the average of the results was taken as the final outcome.

#### **Experiment on cloning formation**

The cell count for each group should be determined prior to processing, with 300 cells to be inoculated per well in a 6-well plate, or 500 cells per well in the MP-HJ-1b experiment. The cells should be cultured for an appropriate number of days in a humidified CO<sub>2</sub> incubator at 37 °C with a CO<sub>2</sub> concentration of 5%. Subsequently, the cells should be washed with 1 $\times$ PBS at room temperature, fixed with 4% paraformaldehyde for 30 min, and then washed again with 1 $\times$ PBS. Following this, the cells should be stained with 0.5% crystal violet under dark conditions for 30 min, washed with 1 $\times$ PBS, and air-dried. Photographs should be taken, and the number of formed clone

colonies should be counted using ImageJ software. The experiment should be repeated 3 times, and the average of the experimental results should be considered as the final outcome.

#### **Immunofluorescence assay**

The cells in each group were enumerated and subsequently seeded into 24-well plates at a density of  $2 \times 10^4$  cells per well. The cells were cultured in a complete medium supplemented with 1% penicillin-streptomycin and 10% FBS, cultured in a humidified atmosphere with 37 °C and 5% CO<sub>2</sub>. Following a PBS wash, the cells were fixed with 4% paraformaldehyde for 30 min, underwent multiple PBS washes, and were then blocked with 5% BSA at room temperature for 1 h. The primary antibody (1:300, Proteintech Group, Inc, 67221-1-Ig) was applied, and the cells were incubated overnight at 4°C. The subsequent day, after a 1-hour incubation at room temperature, the cells were thoroughly washed with PBS. The secondary antibody (1:1000, Proteintech Group, Inc, RGAM004) was added and incubated for 1 h in darkness, followed by additional PBS washes. The cells were sealed with a fluorescence quenching mounting medium containing DAPI (Beyotime biotech co. Ltd, P0131) and imaged under a microscope. The fluorescence intensity of individual cells was quantified using ImageJ software. The experiment was replicated three times, and the mean of the experimental outcomes was considered the final result.

#### **Experiment on the treatment of MP-HJ-1b drug**

MP-HJ-1b is a novel microtubule inhibitor that we designed and reported previously [24]. Con and over-expression cells were divided into drug treatment group and blank control group for the following experiments: cell scratch assay(a total of  $4 \times 10^5$  cells were inoculated per well, the cells were treated with the drug for 24 h after cell adhesion. ), colony formation assay (a total of 500 cells were inoculated per well, the cells were treated with the drug for 8 days after cell adhesion.), transwell assay (a total of  $4 \times 10^4$  cells into small chambers containing, medication treatment for 24 h ), Western blot, and immunofluorescence experiments (a total of  $2 \times 10^4$  cells were inoculated per well, the cells were treated with the drug for 24 h after cell adhesion.), All experiments were conducted using high-glucose DMEM, 1% penicillin-streptomycin, and 10% FBS, MP-HJ-1b was added at an additional 25 nM in the drug treatment group, follow the experimental steps mentioned in the text aboveThe experimental group was supplemented with an additional 25 nM MP-HJ-1b, and the rest of the experimental steps were kept strictly the same as the control group, as described in the methodological description earlier in this chapter. The experiments were repeated three times,

and the average of the results was calculated as the final experimental outcome.

### Statistical analysis

All statistical analyses were performed with GraphPad Prism software version 8.02 (RRID: SCR\_002798, [www.graphpad.com/company/](http://www.graphpad.com/company/), USA). The mean values of the quantitative data were reported along with the standard error of the mean. Student's t-test was employed for comparing intergroup comparisons, whereas one-way analysis of variance with Tukey's multiple comparisons was used for comparisons involving more than two groups. Statistical significance was determined at  $P$ -value < 0.05.

## Results

### Characteristics of cuproptosis-related genes in TCGA-glioma

The disruption of copper homeostasis in different cancers leads to an imbalance in copper regulation, significantly contributing to multiple biological mechanisms involved in tumor progression. Of note, copper exerts its pathological influence on cancer by regulating signal transduction pathways via copper-dependent kinase modulation [25]. To investigate the role of cuproptosis in glioma, the TCGA database was used to examine and analyze the expression of 19 CRGs in glioma ( $n=666$ ) and normal tissues ( $n=2642$ ). The findings revealed a significant upregulation ( $P<0.001$ ) in the expression level of NFE2L2, NLRP3, ATP7A, SLC31A1, FDX1, LIAS, LIPT1, LIPT2, DLD, DLAT, PDHA1, MTF1, CDKN2A, DBT, and DLST in glioma. By contrast, ATP7B, PDHB, GLS, and GCSH expression levels were significantly down-regulated ( $P<0.001$ ) in patients with glioma (Fig. 1A). Cancer usually involves gene mutations; therefore, CRGs mutations in patients with glioma were evaluated through the TCGA database. The results showed that CDKN2A, DLD, ATP7A, ATP7B, PDHA1, NLRP3, and PDHB had high mutation rates of 20%, 3%, 2.4%, 1.8%, 1.8%, 1.3%, and 1%, respectively (Fig. 1B). It is worth noting that CDKN2A, also called P16, is the main negative regulator of the P16/cyclin D1/p-RB tumor pathway. P16 protein inhibits the formation of a complex that exhibits kinase activity between cyclin D and CDK4 and blocks the phosphorylation of the Rb protein by the cyclin D-CDK4 complex, thereby stopping the cell cycle [26]. The mutation rate of CDKN2A in patients with glioma was as high as 20%, highlighting the significance of monitoring unregulated cell proliferation resulting from dysregulated cell cycle in glioma. ATP7A and ATP7B were identified as most frequently associated with copper-induced cell death, with a mutation frequency as high as 33%. Research has demonstrated that specific mutations in ATP7A, such as ATP7AT994I and ATP7AP1386S, can lead to distal motor neuropathy [27]. Mutations

in NLRP3 have been identified to be associated with cryopyrin-associated periodic syndrome, resulting in increased IL-1 $\beta$  secretion. In chromophobe renal cell carcinomas, two mutations in PDHB have been discovered: p.Phe222fs\*35 and p.Arg105Leu. By contrast, the mutation rates of DBT, DLST, NFE2L2, SLC31A1, FDX1, DLAT, MTF1, GLS, LIAS, and LIPT2 were <1% and those of LIPT1 and GCSH were 0%. Significant deletions and amplifications predominantly characterized these mutations.

### Prognosis of cuproptosis-related genes in TCGA-glioma

The impact of CRGs on the prognosis of patients with glioma was comprehensively evaluated using the TCGA database. A survival curve analysis was performed by categorizing the patients into high-expression and low-expression groups based on CRGs expression levels. The findings revealed a significant decrease in the OS of patients with glioma exhibiting high NFE2L2, LIPT2, LIPT1, FDX1, DLST, DLD, ATP7A, and DLAT expression compared with those in the low-expression group. Patients exhibiting low PDHA1, GCSH, CDKN2A, and ATP7B expression were associated with poor prognosis (Fig. 2A). Furthermore, the analysis of the risk ratio of patients with glioma based on OS revealed that NFE2L2, ATP7A, SLC31A1, FDX1, LIPT1, LIPT2, DLD, DLAT, and DLST exhibited hazard ratios (HR) >1 ( $P<0.05$ ). Of note, the expression levels of SLC31A1 and FDX1 were significantly increased, exceeding 200%. PDHA1, GCSH, CDKN2A, and ATP7B hazard ratios were all <1 ( $P<0.05$ ). In particular, ATP7B and GCSH expressions were significantly associated, and lower expression levels were correlated with a higher risk of disease progression and death by >50%. Based on the findings from Fig. 2B, these genes may serve as the risk factors of OS in patients with glioma. Higher NFE2L2, ATP7A, SLC31A1, FDX1, LIPT1, LIPT2, DLD, DLAT, and DLST expressions indicated poorer OS. To assess the impact of CRGs on the prognosis of patients with glioma, the correlation between alterations in the expression of these genes and both progression-free survival (PFS) and disease-specific survival (DSS) was assessed. PFS denotes the duration of survival without further deterioration after treatment, whereas DSS represents the proportion of individuals within a research or treatment group who do not succumb to a specific disease within a specified timeframe. According to the PFS curve, patients with high NLRP3, NFE2L2, LIPT2, LIPT1, FDX1, DLST, DLD, DLAT, ATP7A, and SLC31A1 expressions exhibited a significantly shorter PFS following antitumor therapy. By contrast, patients with low PDHA1, GCSH, CDKN2A, and ATP7B expressions demonstrated poorer prognosis after antitumor treatment compared with patients with high expression of these genes (Fig. 3A). These

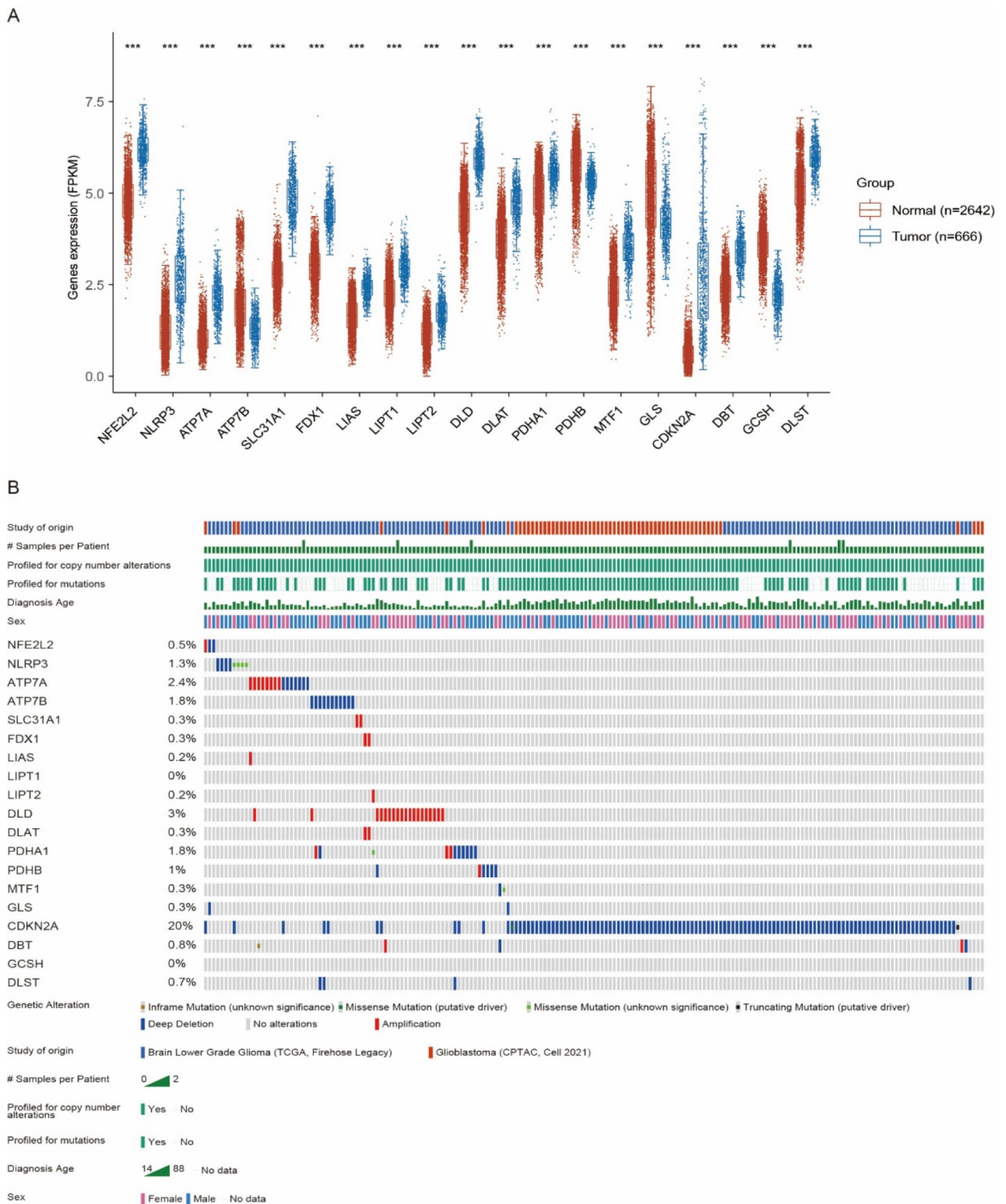


**Fig. 1** Relative expression levels and genetic alterations of CRGs in glioma. **(A)** Expression patterns of CRGs in patients with glioma and healthy individuals. **(B)** Genetic alterations in CRGs with cBioPortal

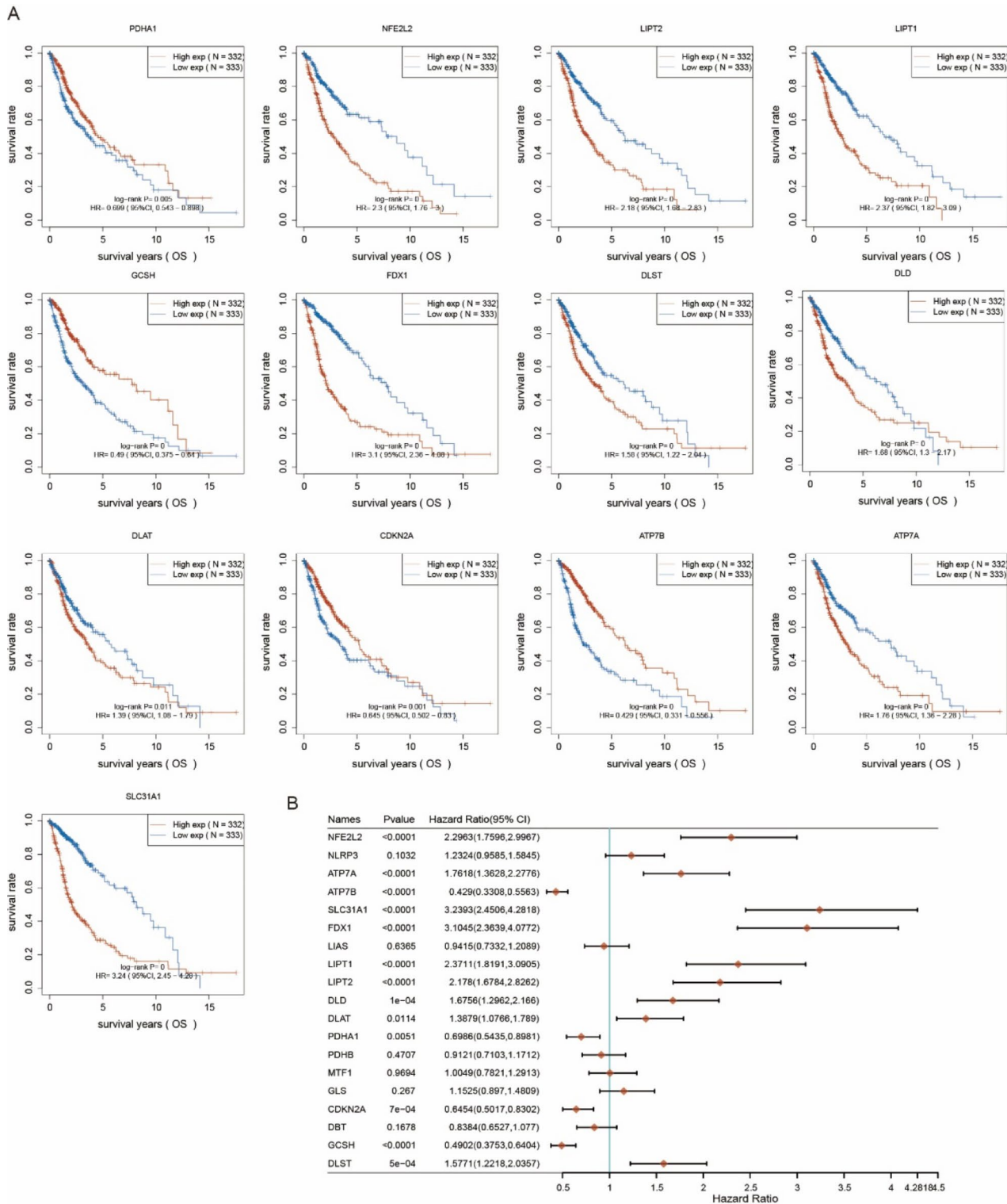


**Fig. 2** OS with respect to CRGs expression in patients with glioma (Kaplan–Meier Plotter). **(A)** OS curves of NFE2L2, LIPT2, LIPT1, FDX1, DLST, DLD, ATP7A, DLAT, PDHA1, GCSH, CDKN2A, and ATP7B. **(B)** HR of CRGs regarding OS of patients with glioma

A

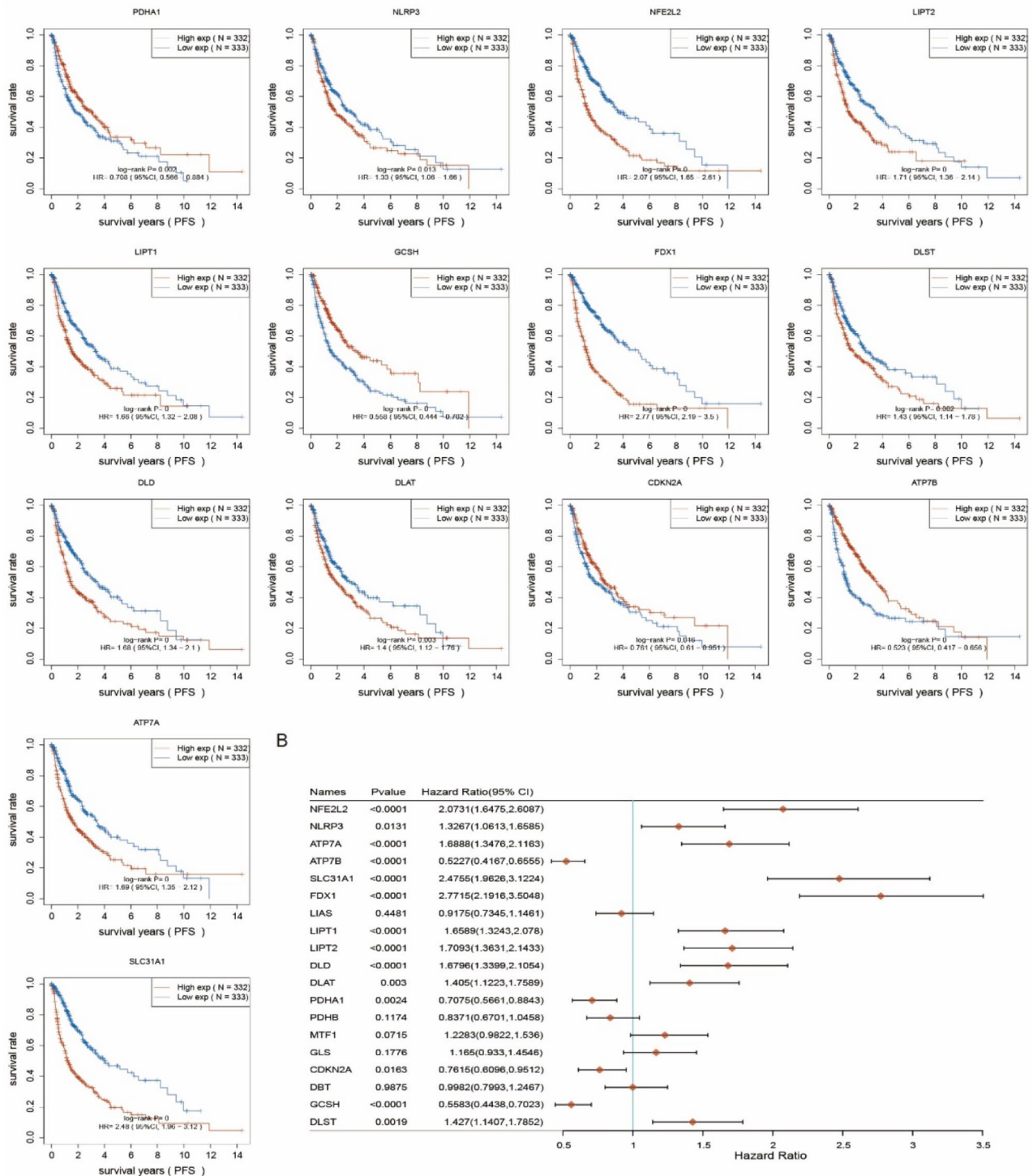


**Fig. 3** PFS with respect to CRGs expression in patients with glioma (Kaplan–Meier Plotter). **(A)** PFS curves of NLRP3, NFE2L2, LIPT2, LIPT1, FDX1, DLST, DLD, DLAT, ATP7A, SLC31A1, PDHA1, GCSH, CDKN2A, and ATP7B. **(B)** HR of CRGs regarding PFS of patients with glioma

findings enabled the assessment of the risk ratio associated with PFS in this population. The results indicated that NFE2L2, NLRP3, ATP7A, SLC31A1, FDX1, LIPT1, LIPT2, DLD, DLAT, DLST, ATP7B, and GCSH were the risk factors of glioma progression (Fig. 3B). Of note, SLC31A1 and FDX1 upregulation was associated with a >140% increase in the risk of disease progression and mortality. By contrast, ATP7B and GCSH downregulation led to a >40% increase in disease progression and mortality risk.

The examination of alterations in CRGs expression and DSS indicated that patients with increased NLRP3, NFE2L2, LIPT2, Lipt1, FDX1, DLST, DLD, DLAT, ATP7A, and SLC31A1 expressions had unfavorable prognosis. Moreover, patients with reduced PDHA1, GCSH, CDKN2A, and ATP7B expressions were linked to poorer prognosis. Based on the HR analysis of DSS, NFE2L2, NLRP3, ATP7A, SLC31A1, FDX1, LIPT1, LIPT2, DLD, DLAT, DLST, ATP7B, and GCSH were the risk factors of DSS in patients with glioma (Fig. 4A). The expression of SLC31A1 and FDX1 was significantly increased, resulting in a >200% increase in the risk of disease progression and death (Fig. 4B). However, the decreased expression of ATP7B and GCSH was associated with a risk increase of >50% in terms of disease progression and death. Furthermore, the hazard risk analysis of OS, PFS, and DSS revealed that the high SLC31A1, FDX1, DLST, LIPT1, LIPT2, DLD, NFE2L2, ATP7A, and DLAT expressions were the statistically significant risk factors of OS, PFS, DFS, and DSS ( $P < 0.05$ ). However, it is noteworthy that low GCSH and ATP7B expressions exhibited statistically significant protective effects on OS, PFS, DFS, and DSS ( $P < 0.05$ ). These findings provide a solid basis for developing a future risk assessment model. In summary, the 11 genes, particularly the elevated expression of SLC31A1 and FDX1 that significantly increased the risk of disease progression and mortality by >200%, were associated with the prognosis of patients with glioma.

#### Prognostic model of 11 cuproptosis-related genes in TCGA-glioma

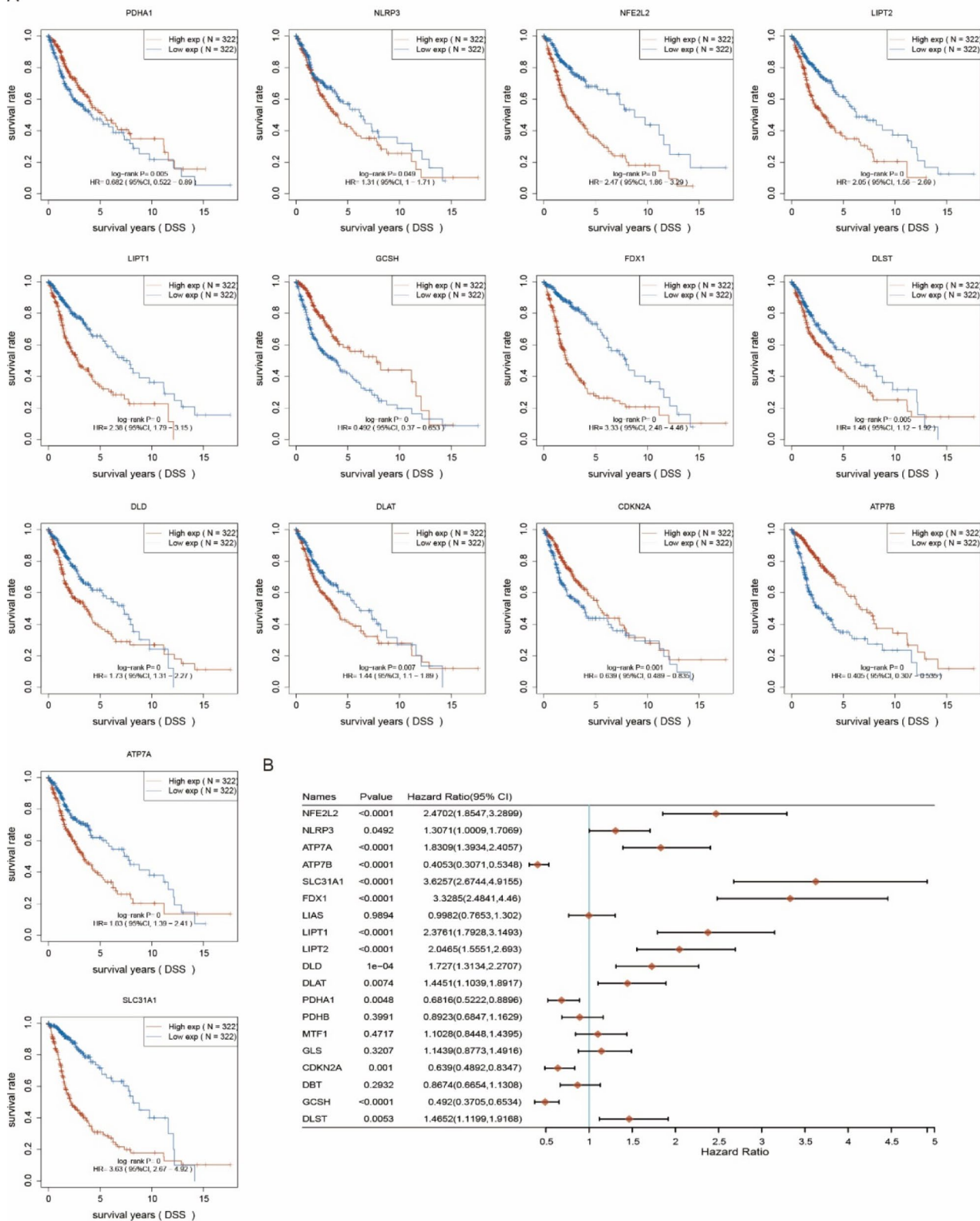
The expression levels of SLC31A1, FDX1, DLST, LIPT1, LIPT2, DLD, NFE2L2, ATP7A, DLAT, GCSH, and ATP7B were found to be significantly correlated with OS, DFS, and DSS in glioma. These 11 genes were incorporated into a multivariate Cox proportional hazard regression model, utilizing data from 666 glioma patients. The parameter  $\lambda$  was ascertained through cross-validation, with a lambda.min of 0.0093 applied in this research. To avoid overfitting, the variable optimization model was refined using Lasso regression, excluding ATP7A (Fig. 5A and B). A risk score was calculated for each patient using the root model, which includes a RiskScore formula incorporating multiple genes with allocated weights

(negative values represent protective genes, while positive values represent risk genes). Patients were classified into high-risk and low-risk categories based on the median risk score. Scatter plots were created to display the distribution of risk values and survival time, and a heatmap was designed to show the expression of signature genes. The scatter plot with survival time indicated that the low-risk group on the left had a marginally longer survival time than the high-risk group on the right, with a higher number of deaths observed in the latter. This strongly suggests a poor prognosis for the high-risk group, highlighting the potential prognostic capability of the 10 genes included in the study. The heatmap displaying the expression of signature genes showed a significant increase in SLC31A1 and FDX1 expressions in the high-risk group. In contrast, the high-risk group demonstrated a significant decrease in expression level compared to the low-risk group. This suggests that SLC31A1, FDX1, GCSH, and ATP7B may have superior prognostic potential (Fig. 5C). A Kaplan–Meier survival curve was utilized to evaluate the difference in prognosis between the high- and low-risk groups. The results revealed a significant difference in OS between the two groups, with the high-risk group demonstrating significantly lower OS (log-rank  $P < 0.05$ ) and a hazard risk > 1 compared to the low-risk group. This validates the influence of the 10 genes on prognosis and their potential prognostic capacity (Fig. 5D). To evaluate the predictive performance of the model, receiver operating characteristic curves were created, and OS at 1, 3, and 5 years was analyzed. The results showed that all three models had an area under the curve (AUC) of >0.8, with the AUC for 1-year OS being the highest. This suggests that the model is highly sensitive in predicting glioma prognosis (Fig. 5E).

#### Relationship between tumor mutational burden (TMB) and cuproptosis-related genes in glioma

TMB is a quantitative measure of the total number of mutations present in cancer. A higher TMB corresponds to an increased abundance of tumor antigens on the surface of cells. These novel antigens, which possess immunogenic properties, are presented to T cells via the major histocompatibility complex protein, thereby triggering an immune response against tumor cells. Thus, TMB holds significant potential as a biomarker for prognosticating the efficacy of tumor immunotherapy. In general, increased TMB levels are associated with heightened sensitivity to immunotherapeutic interventions [28]. To elucidate the influence of CRGs on TMB levels, the relationship between CRGs and TMB was investigated. The results demonstrated a positive correlation between the expression levels of DLAT, DLD, LIPT2, LIPT1, SLC31A1, FDX1, DLST, ATP7A, and NFE2L2 and TMB in glioma (Fig. S1). Conversely, the expression levels

A



B

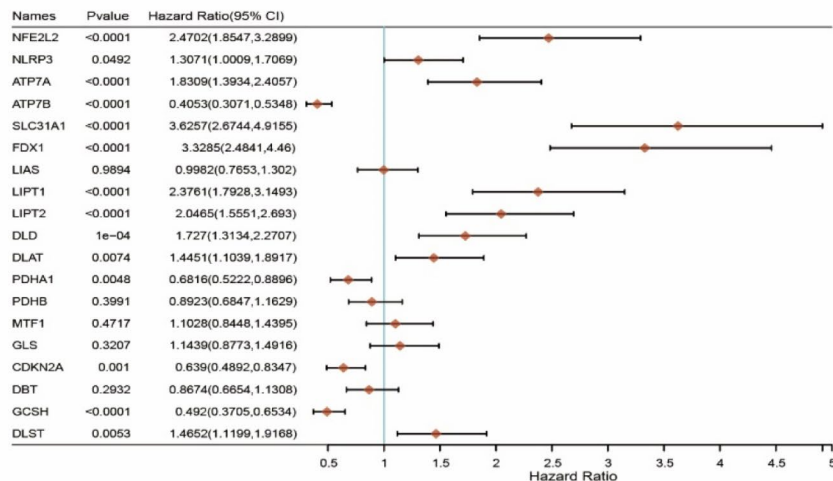


**Fig. 4** DSS with respect to CRGs expression in patients with glioma (Kaplan–Meier Plotter). **(A)** DSS curves of NLRP3, NFE2L2, LIPT2, LIPT1, FDX1, DLST, DLD, DLAT, ATP7A, SLC31A1, PDHA1, GCSH, CDKN2A, and ATP7B. **(B)** HR of CRGs regarding DSS of patients with glioma

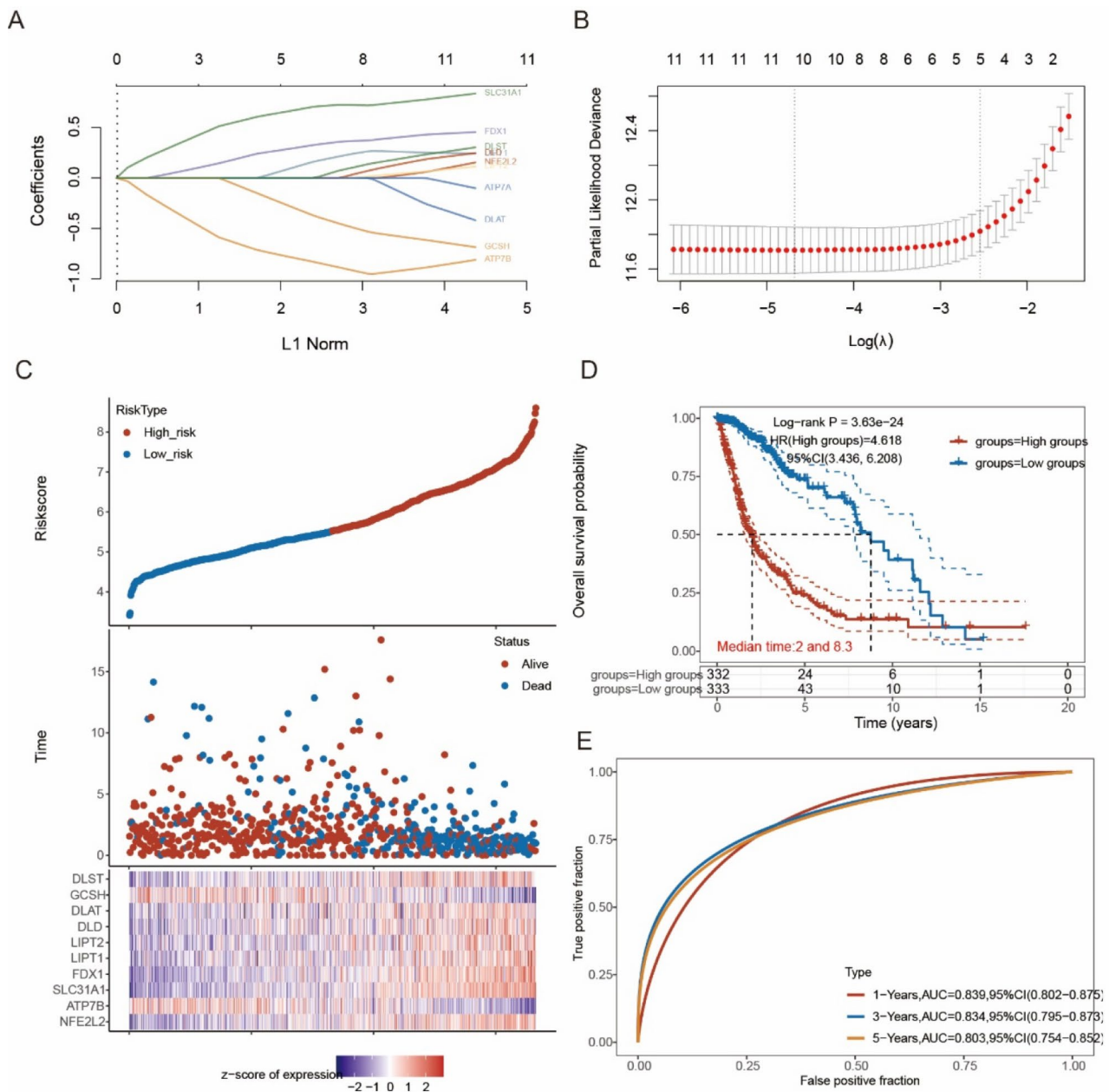


**Fig. 5** Advanced Prognosis Model Analysis of 11 CRGs in Patients with Glioma (**A-B**) Coefficients of selected features are shown using the lambda parameter. The abscissa represents the lambda value and the ordinate represents the coefficients of the independent variable. (**C**) RiskScore, survival time, and survival status of the selected dataset. The top scatter plot represents the RiskScore from low to high, with different colors indicating different groups. The scatter plot distribution illustrates the RiskScore of different samples corresponding to the survival time and survival status. The bottom heatmap shows the gene expression of the signature. (**D**) Kaplan–Meier survival analysis of the risk model from the dataset. The different groups were compared using the log-rank test. HR (High exp) represents the hazard ratio of the low-expression samples relative to the high-expression samples. HR > 1 indicates that the gene is a risk factor, and HR < 1 indicates that the gene is a protective factor. HR (95% CI) and the median survival time (LT50) for different groups are shown in years. (**E**) ROC curve and AUC of the genes. Higher AUC values indicate higher predictive power

of ATP7B and GCSH were negatively correlated with TMB in glioma. NLRP3 was employed as a control, and the results suggested that the aforementioned CRGs (DLAT, DLD, LIPT2, LIPT1, SLC31A1, FDX1, DLST, ATP7A, NFE2L2, ATP7B, and GCSH) have the potential to function as noninvasive screening markers for glioma

assessment via pathological biopsy prior to TMB estimation. Furthermore, these genes may provide additional reference value for evaluating the sensitivity of glioma to immunotherapy.

### Role of cuproptosis-related genes in glioma TME regulation

TME is complex and changeable with regard to its interaction with tumor cells. In TME, several immune cells are integral components, such as T cells, B cells, macrophages. Tumor-associated macrophages (TAMs) undergo a series of metabolic reprogramming processes, including glucose metabolism and glutamine and fatty acid metabolism, among others. The metabolic reprogramming of TAMs provides nutritional support for tumor cells, and maintaining an immunosuppression phenotype promotes tumor progression [29, 30]. To comprehend the interplay among copper-induced cell death, inflammatory response, and glioma, two immunoassays (MCP counter) were performed to examine the association between CRGs and immune cell infiltration in patients with glioma. The results revealed that ATP7A exhibited the most robust positive correlation with B cell immune infiltration. However, GCSH was significantly negatively correlated with B cell immune infiltration. The immune infiltration of macrophages was positively correlated with NFE2L2, FDX1, and ATP7A and negatively correlated with GCSH and ATP7B. In the case of myeloid dendritic cell infiltration, a strong positive correlation was detected with NFE2L2 and FDX1, with the highest negative correlation with ATP7B. In the context of neutrophil infiltration, NFE2L2, FDX1, and ATP7A were highly positively correlated, whereas GCSH and ATP7B were strongly negatively correlated. Regarding CD4+ T cell infiltration, DLAT and ATP7B exhibited a slightly stronger negative correlation. In the case of CD8+ T cell infiltration, SLC31A1 exhibited the most pronounced positive correlation. At the same time, GCSH and ATP7B demonstrated a strong negative correlation (Fig. S4A). A positive correlation was observed between SLC31A1, NFE2L2, FDX1, and ATP7A and M1/M2 macrophage infiltration, with a negative correlation with monocyte infiltration (Fig. S4B). GCSH and ATP7B were negatively correlated with M1/M2 macrophage infiltration but positively correlated with monocyte infiltration. Thus, these six genes potentially exert an influence on the process of monocyte transformation and migration from blood to tissues, particularly toward macrophages, via certain signaling pathways. Moreover, they may modulate inflammatory responses, thereby contributing to glioma initiation and progression by influencing the equilibrium between M1 and M2 macrophages.

The top 10 identified genes (COL4A1, TOP2A, LYZ, COL3A1, MYBL2, CD163, CHI3L1, TIMP1, POSTN, and LTF) and CRGs (DLAT, DLD, LIPT2, LIPT1, SLC31A1, FDX1, DLST, ATP7A, NFE2L2, ATP7B, and GCSH) were next analyzed. The results revealed a negative correlation between ATP7B and GCSH and the top 10 significantly upregulated genes. In particular, ATP7B

exhibited a negative correlation with TIMP1, LTF, and CHI3L1, whereas GCSH was negatively correlated with TIMP1, CHI3L1, and CD163. DLAT, DLD, LIPT2, LIPT1, SLC31A1, FDX1, DLST, ATP7A, and NFE2L2 were significantly positively correlated with the top 10 upregulated genes. Of note, SLC31A1 and FDX1 demonstrated significant positive correlations with TOP2A and COL4A1 (Fig. S4C).

### Cuproptosis-related gene, the role of SLC31A1 in glioma patients

To investigate the biological role of SLC31A1 in glioma, we analyzed the glioma tissues with high and low SLC31A1 expression (TCGA database). In glioma, 515 genes were upregulated and 106 genes were downregulated ( $FC > 2$ ,  $P < 0.05$ ). The first 100 genes were selected based on the above differentially expressed genes for further analysis. Epithelial membrane protein 3 (EMP3) is a transmembrane protein that is widely distributed and highly expressed in proliferative cells such as granulocytes, monocytes, lymphocytes, melanocytes, keratinocytes, and fibroblasts, while being expressed at low levels in the brain [31, 32]. However, in wild-type glioma cells, there is an abnormal upregulation of EMP3 expression, which is closely associated with poor prognosis in patients [32]. Studies have demonstrated that EMP3 can enhance the recruitment of TBC1D5, resulting in the inactivation of RAB7 and the inhibition of EGFR degradation in tumor cells [33]. This process promotes EGFR/CDK2 signaling and facilitates cancer cell proliferation. The membrane-associated protein Annexin A1 (ANXA1) has been shown to promote cell proliferation, migration, and invasion by modulating the PI3K-Akt signaling pathway. Stimulation of ANXA1 by TNF- $\alpha$  in the tumor microenvironment leads to increased expression levels, resulting in the activation of the PI3K-Akt signaling pathway. This alteration affects the protein levels of MMP-2/-9, promoting proliferation, invasion, and migration of glioma cells [34]. Secreted frizzled-related protein 2 (SFRP2) functions as a tumor suppressor gene in glioma cells, binding to Wnt ligands or frizzled receptors to regulate Wnt signaling transduction. Acting as an antagonist or agonist of the Wnt signaling pathway, low levels of SFRP2 can act as an activator, leading to increased expression of Wnt/ $\beta$ -catenin pathway-related proteins, promoting cancer cell proliferation, invasion, and migration [35, 36].

Dual-specificity phosphatase 26 (DUSP26) exhibits dual roles in inhibiting and promoting tumorigenesis in different environments. Lower levels of DUSP26 can excessively activate certain proteins in the MAPK and Akt signaling pathways, including p38, STAT1, ERK, YAP, Akt, and AMPK, inhibiting cancer cell apoptosis and promoting proliferation and migration [37–39].

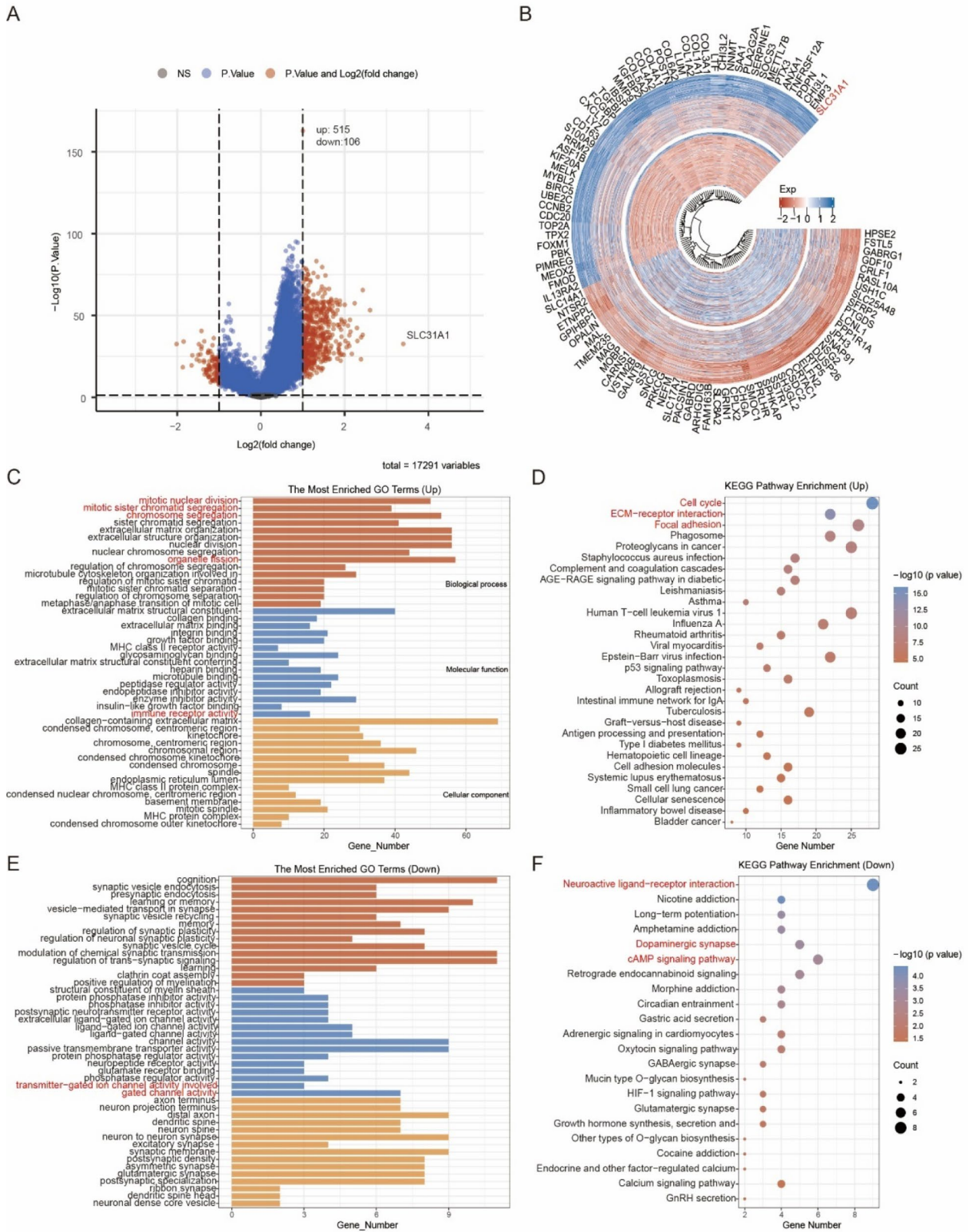


**Fig. 6** (See legend on next page.)

(See figure on previous page.)

**Fig. 6** Functional analysis of differentially expressed SLC31A1 in gliomas. **(A)** Volcano Plot: Transcriptomic data from 66 glioma tissue in TCGA database were utilized to analyze the transcriptome profiles of SLC31A1 with high and low expression levels. The volcano plot was generated based on fold change and adjusted p-values ( $p < 0.05$ ,  $FC > 2$ ). Significantly upregulated genes are denoted by red dots, downregulated genes by blue dots, and genes with no significant difference by gray dots. **(B)** Heatmap: The heatmap illustrates the expression patterns of differentially expressed genes across various tissues, with distinct colors representing diverse expression trends. To manage the extensive list of differentially expressed genes, only the top 100 upregulated and top 100 downregulated genes with the most significant changes were displayed. **(C-F)** Functional Enrichment: KEGG pathway enrichment analysis was conducted for both upregulated and downregulated genes, whereas GO term enrichment analysis was performed separately for upregulated and downregulated genes. The functional enrichment analyses were performed using the R package ClusterProfiler (version 3.18.0). In the results, varying colors indicate the significance of the enrichment outcomes, with larger values corresponding to smaller FDR values. The size of the circles on the plot represents the number of enriched genes, with darker circles indicating a greater number of enriched genes

Protein kinase C and casein kinase substrate in neurons 1 (PACSIN1) plays a crucial role as a peripheral membrane protein in synaptic vesicle transport cycles and receptor-mediated endocytosis. In glioma cells, PACSIN1 expression gradually decreases with the severity of glioma grading, and lower PACSIN1 expression is associated with poorer patient survival [40].

Cell cycle progression and epithelial-mesenchymal transition (EMT) are critical steps in tumor progression. Transcription factors MYBL2 and Forkhead box M1 (FoxM1), known as cell cycle proliferation factors, are co-expressed and overexpressed in glioma cells. Studies have revealed that the overexpression of MYBL2 and FoxM1 leads to increased expression of cell cycle-related proteins such as cyclin B, cyclin D, N-cadherin, and Vimentin, promoting cell proliferation and differentiation. MYBL2 acts downstream of the FoxM1/Akt signaling pathway, where Akt activation in glioma cells promotes the expression of FoxM1 and MYBL2 genes, resulting in excessive proliferation, invasion, and migration of glioma cells [41, 42].

A systematic cluster analysis was next performed (Fig. 6C and F). The upregulated and downregulated genes were examined through KEGG and GO analyses. The KEGG analysis of upregulated genes revealed that the biological functions of CRGs encompassed numerous pathogenic infections, inflammatory reactions, ECM–receptor interactions, cell cycle processes, and phagocytosis. Among these categories, the enrichment rate of CRGs in ECM–receptor interaction, cell cycle, and phagocytosis was statistically significant. Of note, the highest enrichment rate was observed within the cell cycle (Fig. 6D). The GO analysis of upregulated genes revealed that CRGs were significantly associated with mitotic nuclear division, chromosome segregation, organelle fission, nuclear division, extracellular structure organization, and ECM organization, all of which were statistically significant. Among the latter four categories, the CRGs exhibited the highest enrichment rate (Fig. 6E). The aforementioned signaling pathways are frequently observed in tumors and significantly associated with tumor cell proliferation, TME, and inflammatory responses. These findings imply that CRGs may play a role in glioma initiation and progression by

influencing tumor cell proliferation, TME, and inflammatory responses. The KEGG analysis of downregulated genes revealed that CRGs exhibited the highest enrichment rate in the neuroactive ligand–receptor interaction pathway, with statistical significance. Additionally, these genes were highly significant in nicotine addiction (Fig. 6E). Furthermore, the GO analysis of downregulated genes indicated that CRGs were significantly enriched in vesicular-mediated transport in synapses (Fig. 6E and F).

#### The expression level of SLC31A1 significantly influences GBM

To investigate the impact of the copper transporter gene SLC31A1 on the proliferation, migration, and invasion capabilities of glioma cells, we generated stable transfected cell lines with SLC31A1 overexpression (Over-expression-SLC31A1) and corresponding control (Vector) group. The successful establishment of stable transfected cell lines was confirmed through qRT-PCR and Western blot analysis. Our findings demonstrated a significant increase in RNA and protein expression levels in the Over-expression-SLC31A1 group, and a notable decrease in RNA and protein expression levels in the shRNA-SLC31A1 group (Fig. 7A–B). Immunofluorescence analyses of cells from each group revealed a positive correlation between SLC31A1 expression levels and individual cell fluorescence intensity (Fig. 7C). The results of CCK-8 assays revealed that reduced SLC31A1 expression led to a decelerated cell proliferation rate, whereas elevated SLC31A1 expression significantly accelerated cell proliferation (Fig. 7D). Furthermore, Transwell, colony formation, and scratch assays showed that overexpression of SLC31A1 promoted the invasion, migration, and colony-forming ability of glioma cells, whereas downregulation of SLC31A1 expression significantly inhibited these capabilities (Fig. 7E–G).

#### The microtubule inhibitor MP-HJ-1b may suppress the proliferation, invasion, and migration of glioma cells by downregulating the expression of SLC31A1

MP-HJ-1b, a colchicine binding site inhibitor, has been demonstrated to inhibit the proliferation of various tumor cells. However, the impact of MP-HJ-1b on GBM cell proliferation has not yet been documented. In this

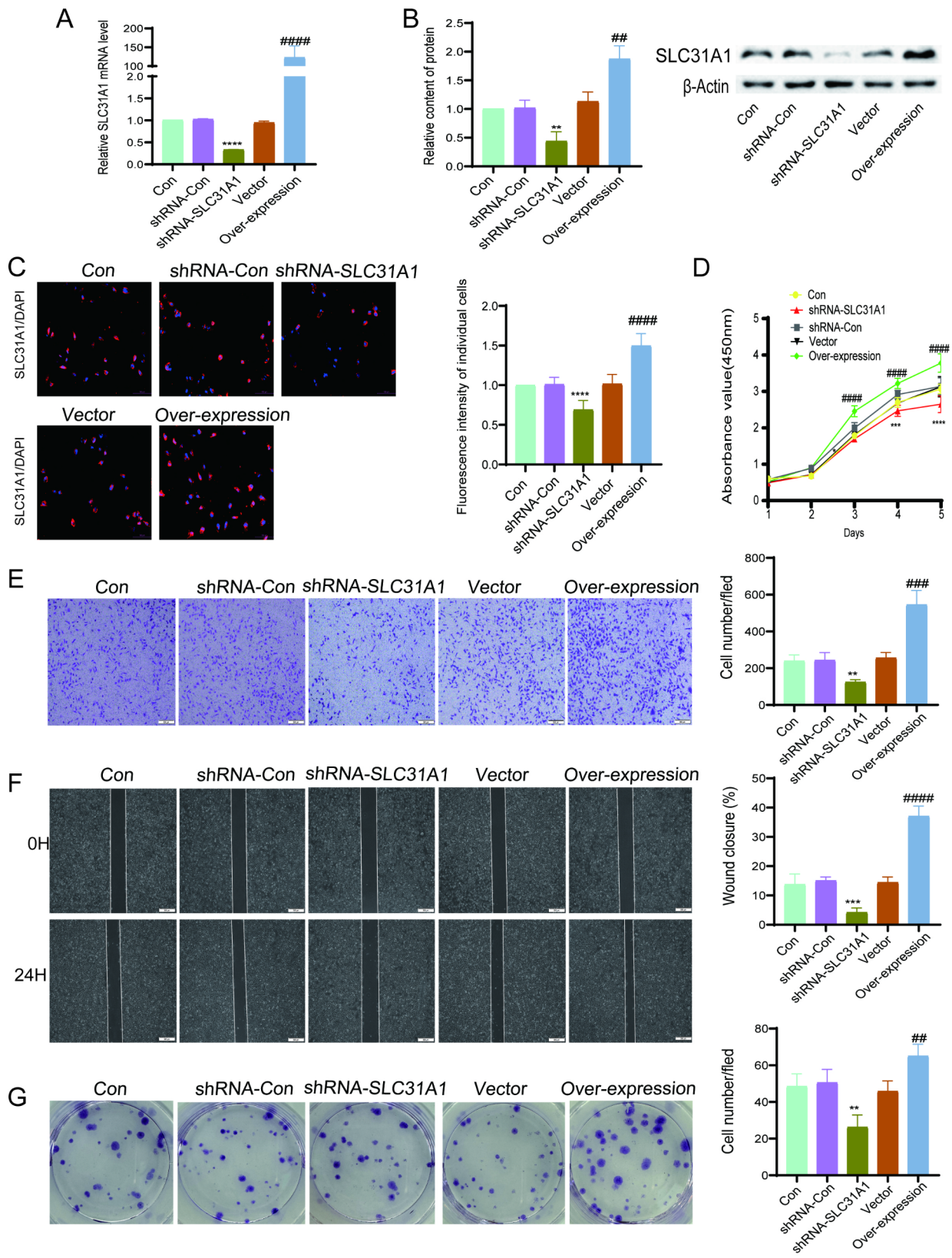


**Fig. 7** (See legend on next page.)

(See figure on previous page.)

**Fig. 7** Enhanced Expression of SLC31A1 Gene Promotes Proliferation, Metastasis, and Invasion in GBM. **(A)** RT-PCR validation of differential SLC31A1 mRNA expression between shRNA-SLC31A1 cells and over-expression cells. **(B)** Western blot validation of varying SLC31A1 protein expression levels among distinct stable transfection cell lines. **(C)** Immunofluorescence validation of the impact of high and low SLC31A1 expression levels on protein expression. The results demonstrate that the fluorescence intensity of individual cells in the SLC31A1 interference group is lower than that of the control group, whereas the fluorescence intensity of individual cells in the SLC31A1 overexpression group is higher than that of the control group. Each bar represents the mean  $\pm$  SEM of three independent experiments. Compared to the vector group, #####  $p < 0.0001$ ; compared to shRNA-Con, \*\*\*\* $p < 0.0001$ . **(D)** CCK-8 assay assessing the influence of SLC31A1 expression levels on cell proliferation in LN229 cells. Reduced SLC31A1 expression leads to a significant decrease in cell proliferation, whereas elevated SLC31A1 expression enhances proliferation. **(E)** Transwell assay illustrating that SLC31A1 overexpression notably enhances the invasion capability of cells LN229. **(F)** Scratch assay evaluating the impact of SLC31A1 expression levels on the migration ability of LN229 cells. LN229 cells with heightened SLC31A1 expression exhibit significantly improved migration ability. **(G)** Colony formation assay confirming the disparity in colony formation ability in LN229 cells due to varying SLC31A1 expression levels. Cells with low SLC31A1 expression display diminished colony formation ability, whereas high SLC31A1 expression fosters colony formation. Each bar represents the mean  $\pm$  SEM of three independent experiments. Compared to Vector, ## $p < 0.01$ , ### $p < 0.001$ , #### $p < 0.0001$ ; compared to shRNA-Con, \*\* $p < 0.01$ , \*\*\* $p < 0.001$ , \*\*\*\* $p < 0.0001$

study, we investigated the influence of MP-HJ-1b on the expression of the SLC31A1 gene in LN229 cells and LN229 cells with SLC31A1 overexpression. Immunoblotting experiments showed a reduction in the expression of SLC31A1 protein in both LN229 cells and stable transfectants overexpressing SLC31A1 following MP-HJ-1b treatment (Fig. 8A). Moreover, immunofluorescence experiments on MP-HJ-1b-treated cells exhibited a decline in SLC31A1 protein expression (Fig. 8B). To further confirm the potential of MP-HJ-1b to modulate GBM cells through altering SLC31A1 expression, we conducted cell transwell, scratch, and colony formation assays to evaluate cell proliferation, invasion, and migration capabilities. The findings indicated that treatment with MP-HJ-1b resulted in decreased invasion, migration, and colony formation abilities of the cells (Fig. 8C-E). In conclusion, our results propose that MP-HJ-1b might impede GBM cell proliferation, invasion, and migration abilities by suppressing the expression of the SLC31A1 gene.

## Discussion

The findings of the present study identified increased expressions of SLC31A1, FDX1, DLST, LIPT1, LIPT2, DLD, NFE2L2, ATP7A, and DLAT as statistically significant risk factors ( $P < 0.05$ ) for glioma prognosis. Additionally, reduced expressions of GCSH and ATP7B were also identified as risk factors for glioma prognosis. Overall, these 11 genes were associated with the prognosis of patients with glioma, particularly the increased expression of SLC31A1 and FDX1, which were associated with a greater than 200% increase in the risk of disease progression and mortality. Previous studies have demonstrated that abnormal expression of CRGs is not only significantly associated with lower OS in patients, but also closely related to tumor immune infiltration [43]. Immune cells infiltrate the tumor microenvironment, where tumor cells promote immune escape by overexpressing immune checkpoint proteins, including PD-L1, CTLA-4, and CD47. These proteins subsequently suppress T cell activation and impair macrophage phagocytic activity [44, 45]. Li demonstrated that the expression

levels of CRGs (e.g., FDX1, DLAT, and DLD) in GBM are significantly correlated with the expression of immune checkpoint proteins, potentially contributing to the formation of an immunosuppressive microenvironment in GBM [46]. Our analysis of tumor-infiltrating immune cells revealed that the abnormal expression of CRGs is closely associated with tumor immune infiltration, primarily disrupting the balance of M1/M2 macrophages. This imbalance modulates inflammatory responses and contributing to glioma initiation and progression.

TMB is a quantitative measure of the total number of mutations present in cancer. CRGs (e.g., CDKN2A, PDHB, and ATP7B) exhibit varying degrees of genetic mutations and DNA methylation across different cancer types. Mutations in CRGs disrupt intracellular copper homeostasis, leading to oxidative stress and impairment of the tricarboxylic acid (TCA) cycle. These effects subsequently cause DNA damage and compromise the DNA damage repair system, thereby increasing TMB levels [47–49]. Meanwhile, alterations in the methylation levels and genetic mutations of SLC31A1 have been observed in various cancers, indicating a potential correlation between SLC31A1 and TMB [50]. In glioma cells, our study also identified a potential link between CRGs and TMB. Specifically, the expression levels of CRGs, including FDX1, SLC31A1, ATP7A, and others, were found to be positively correlated with TMB, whereas the expression levels of ATP7B and GCSH demonstrated a negative correlation with TMB. Our findings suggest that CRGs have the potential to serve as non-invasive screening biomarkers and indicators for assessing immunotherapy sensitivity.

The interaction between copper ions and various proteins regulates copper homeostasis. The plasma membrane protein SLC31A1 is responsible for the cellular uptake of copper in the  $\text{Cu}^{2+}$  ion form. Intracellular transportation of copper to specific target proteins or organelles, such as superoxide dismutase 1 (SOD1) and cytochrome c oxidase (COX) in the mitochondria, as well as ATP7A/B in the trans-Golgi network (TGN), is facilitated by chaperons (CCS, COX17, and ATOX1). Meanwhile, ATP7A/B plays a crucial role in loading copper

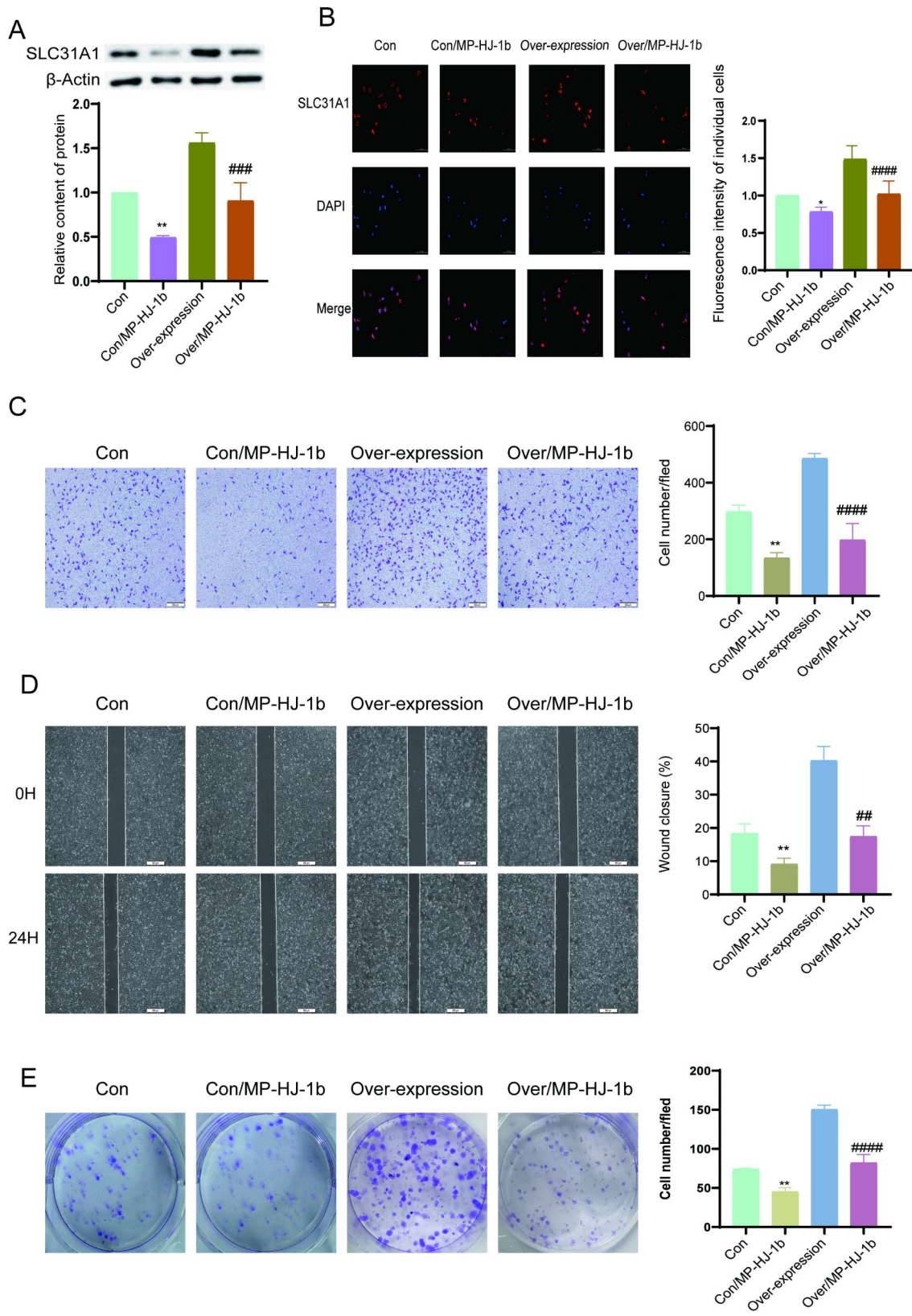


**Fig. 8** (See legend on next page.)

(See figure on previous page.)

**Fig. 8** MP-HJ-1b Reduces SLC31A1 Expression and Suppresses Proliferation, Invasion, and Migration Abilities of LN229 Cells. **(A)** Significant reduction in SLC31A1 protein expression in LN229 cells after treatment with MP-HJ-1b. **(B)** Immunofluorescence Validation of the effect of MP-HJ-1b on SLC31A1 Protein Expression. The results demonstrate that both LN229 cell group and over-expression cell group exhibit decreased expression of SLC31A1 protein after treatment with MP-HJ-1b. Each bar represents the mean  $\pm$  SEM of three independent experiments. Compared to over-expression, ####  $p < 0.0001$ ; compared to Con, \* $p < 0.05$ . **(C)** Transwell assay demonstrates the inhibitory effect of MP-HJ-1b on the invasion ability of LN229 cells. **(D)** Scratch assay indicates a notable decrease in the migration ability of cells treated with MP-HJ-1b. **(E)** Colony formation assay shows that MP-HJ-1b significantly inhibits the colony formation ability of LN229 cells. Each bar represents the mean  $\pm$  SEM of three independent experiments. Compared to the over-expression, the over-expression-MP-HJ-1b group exhibits significant statistical differences, ## $p < 0.01$ , ### $p < 0.001$ , #### $p < 0.0001$ ; compared to the LN229 group, the LN229-MP-HJ-1b group show significant statistical differences, \* $p < 0.05$ , \*\* $p < 0.01$

onto copper-dependent enzymes. It utilizes the energy derived from ATP hydrolysis to transport copper from TGN to the plasma membrane, thereby promoting copper excretion in response to increased intracellular copper levels [51–54]. In the present study elevated ATP7A levels were associated with poor glioma prognosis, suggesting a potential role in promoting copper loading onto copper-dependent enzymes.

Therapeutic strategies targeting copper metabolism in tumors can be classified into two primary categories: (i) copper ionophores, which induce cytotoxic effects by elevating of intracellular copper concentrations. For example, the Elesclomol-Cu<sup>2+</sup> complex is transported to the mitochondria and accumulated within cells. This accumulation leads to the reduction of Cu<sup>2+</sup> to Cu<sup>+</sup>, generating reactive oxygen species (ROS) and depleting glutathione levels, ultimately killing melanoma and leukemia cells [55]. (ii) In contrast, copper chelators exert antitumor effects by reducing intracellular copper levels. For example, a nanoparticle system loaded with di-2-pyridylketone-4,4-dimethyl-3-thiosemicarbazone(Dp44mT) can effectively target the blood-brain barrier and GBM multiforme, demonstrating significant therapeutic efficacy [56]. Notably, the copper chelator TTM exhibits inhibitory effects on BRAFV600E-mutated cells (HT-29), while demonstrating contrasting effects in BRAF wild-type (HCT-116) cells [57]. Relevant studies have shown that the effect of the copper chelator ammonium tetrathiomolybdate (ATTM) on the proliferation of lung adenocarcinoma cells is concentration-dependent, with low concentrations promoting proliferation and high concentrations inhibiting it [58]. Current research indicates that copper-based therapeutic strategies require precise selection based on tumor type and genetic background.

Compared to other tumors, glioblastoma (GBM) is characterized by distinct biological features, including the blood-brain barrier, pronounced tumor heterogeneity, and an immunosuppressive microenvironment. These characteristics make GBM particularly susceptible to alterations in copper homeostasis. This study utilized bioinformatics analysis to identify 11 CRGs (SLC31A1, FDX1, DLST, LIPT1, LIPT2, DLD, NFE2L2, ATP7A, DLAT, GCSH, and ATP7B) as the most promising biomarkers for the diagnosis and treatment of glioblastoma. The roles of these genes in several processes,

including the regulation of angiogenesis, cell apoptosis, cell migration, cell proliferation, and TME in glioma, need to be further explored to elucidate how these CRGs affect glioma progression. Further functional analysis of SLC31A1, which exhibited significant differential expression, revealed its involvement in mitotic and cell cycle regulatory processes.

SLC31A1 is a core transporter regulating cellular copper ion uptake, playing a key role in maintaining copper homeostasis and modulating cuproptosis pathways. Its abnormal expression is closely associated with various diseases, including Wilson's disease, neurodegenerative diseases, and the progression of multiple cancers [59, 60]. Notably, SLC31A1 demonstrates significant tissue specificity across various tumor types. It is highly expressed in breast cancer, esophageal cancer, and colorectal cancer, where its expression correlates with poor prognosis and chemoresistance. In contrast, it is downregulated in cholangiocarcinoma and clear cell renal cell carcinoma [61]. Although the role of SLC31A1 has been extensively studied in various tumors, its function and mechanisms in glioma remain poorly explored. This study demonstrated that upregulation of SLC31A1 expression promotes glioma cell proliferation and migration capabilities, whereas SLC31A1 knockdown markedly suppresses these oncogenic processes. These findings suggest that SLC31A1 may play a significant role in the pathogenesis and progression of glioma.

Intriguingly, analogous to iron ions, copper ions participate in Fenton-like reactions, leading to the generation of hydroxyl radicals. The excessive intracellular accumulation of copper in cancer cells results in substantial reactive oxygen species (ROS) production, thereby initiating a distinct form of regulated cell death known as cuproptosis. This novel cell death mechanism offers promising therapeutic potential for cancer treatment [59, 60]. The microtubule inhibitor MP-HJ-1b, previously developed by our research team, specifically targets the colchicine-binding site and induces ferroptosis through multiple mechanisms, including the downregulation of SLC7A11 and glutathione peroxidase 4 (GPX4) expression, depletion of intracellular glutathione levels, and subsequent accumulation of lipid ROS [24]. Our study found that MP-HJ-1b can significantly inhibit the expression of SLC31A1 in glioma cells, thereby effectively suppressing

their proliferative and migratory capabilities. These findings suggest the potential value of SLC31A1 as a therapeutic target. This study highlights the critical role of copper metabolism regulatory networks in cancer therapeutics, revealing two distinct therapeutic strategies: targeting SLC31A1 to potentiate chemosensitivity through copper metabolism modulation; and utilizing MP-HJ-1b demonstrates multi-target therapeutic effects by simultaneous regulation of both ferroptosis and cuproptosis pathways.

This study has the following limitations. First, selection bias in public databases may affect the robustness of the analysis. Second, validation of drug mechanisms is currently limited to the cellular level and requires further evaluation through animal models and clinical trials to assess their efficacy and safety. Previous studies have consistently demonstrated that targeted inhibition of the SLC31A1 gene effectively suppresses tumor proliferation and metastatic progression in mouse models of both breast cancer and non-small cell lung cancer (NSCLC) [62, 63]. These findings provide a theoretical basis for the clinical translation of CRGs-targeted therapies. However, CRGs-targeted therapy still faces multiple challenges. For instance, the therapeutic efficacy of CRGs-targeted therapies is easily influenced by the tumor microenvironment and tumor heterogeneity, which contribute to the limitations of single gene-targeted therapies. Therefore, combining CRGs-targeted therapies with immune checkpoint inhibitors or chemotherapy agents through multi-pathway synergism is considered a promising future direction in cancer treatment.

#### Abbreviations

TMZ	Temozolomide
COX	Cytochrome c oxidase
CTR1/SLC31A1	Copper transporter 1
CRGs	Cuproptosis-related genes
TTM	Tetrathiomolybdate
VEGF	Vascular endothelial growth factor
DFS	Disease-free survival
OS	Overall survival
RFS	Recurrence-free survival
GO	Gene Ontology
KEGG	Kyoto Encyclopedia of Genes and Genomes
NCI	National Cancer Institute
ATCC	American Type Culture Collection
DMEM	Dulbecco's Modified Eagle Medium
FBS	Fetal bovine serum
HR	Risk ratios
PFS	Progression-free survival
DSS	Disease-specific survival
TMB	Tumor mutational burden
TME	Tumor microenvironment
TAM	Tumor-associated macrophages
EMP3	Epithelial membrane protein 3
ANXA1	Annexin A1
SFRP2	Secreted frizzled-related protein 2
DUSP26	Dual-specificity phosphatase 26
Dp44mT	Di-2-pyridylketone-4,4-dimethyl-3-thiosemicarbazone
ATTM	Ammonium tetrathiomolybdate
PACSLIN1	Protein kinase C and casein kinase substrate in neurons 1

EMT	Epithelial–mesenchymal transition
FoxM1	Forkhead box M1
ECM	Extracellular matrix
ROS	reactive oxygen species

#### Supplementary Information

The online version contains supplementary material available at <https://doi.org/10.1186/s12885-025-14151-7>.

Supplementary Material 1

Supplementary Material 2

#### Acknowledgements

We are grateful to Xiaozhen Ma and Mi Li for their help with the funding, and we extend our heartfelt thanks to editor and anonymous reviewers for their efforts in reviewing and commenting on our research.

#### Author contributions

YW, HMW, SQ, and PW analyzed the results. JHD, ML, XZM, and HMW contributed research materials. SQ, JHD and HMW designed the research and wrote the manuscript. All authors contributed to the article and approved the submitted version.

#### Funding

This work was financially supported by the Key Scientific Research Program of the Shaanxi Provincial Department of Education (22JS004, 23JS009) and the Research and Development Fund of the Affiliated Hospital of Shandong Second Medical University(2024FYM038).

#### Data availability

The datasets presented in this study can be found in online repositories. The original contributions presented in the study are included in the article/ Supplementary Materials.

#### Declarations

#### Ethics approval and consent to participate

Not applicable.

#### Consent for publication

Not applicable.

#### Competing interests

The authors declare no competing interests.

#### Supplementary Material

The Supplementary Material for this article can be found online at: <https://www.>

#### Clinical trial

Not applicable.

Received: 11 November 2024 / Accepted: 14 April 2025

Published online: 12 May 2025

#### References

- Sung H, Ferlay J, Siegel RL, Laversanne M, Soerjomataram I, Jemal A, Bray F. Global Cancer statistics 2020: GLOBOCAN estimates of incidence and mortality worldwide for 36 cancers in 185 countries. *CA Cancer J Clin.* 2021;71:209–49.
- Schaff LR, Mellingshoff IK. Glioblastoma and other primary brain malignancies in adults: A review. *JAMA.* 2023;329:574–87.
- Ma R, Taphoorn MJB, Plaha P. Advances in the management of glioblastoma. *J Neurol Neurosurg Psychiatry.* 2021;92:1103–11.

4. Lefranc F, Le Rhun E, Kiss R, Weller M. Glioblastoma quo Vadis: will migration and invasiveness reemerge as therapeutic targets? *Cancer Treat Rev*. 2018;68:145–54.
5. Balca-Silva J, Matias D, Carmo AD, Sarmento-Ribeiro AB, Lopes MC, Moura-Neto V. Cellular and molecular mechanisms of glioblastoma malignancy: implications in resistance and therapeutic strategies. *Semin Cancer Biol*. 2019;58:130–41.
6. Festa RA, Thiele DJ. Copper: an essential metal in biology. *Curr Biol*. 2011;21:R877–883.
7. Tsvetkov P, Coy S, Petrova B, Dreishpoon M, Verma A, Abdusamad M, Rossen J, Joesch-Cohen L, Humeidi R, Spangler RD, Eaton JK, Frenkel E, Kocak M, Corsello SM, Lutsenko S, Kanarek N, Santagata S, Golub TR. Copper induces cell death by targeting lipoylated TCA cycle proteins. *Science*. 2022;375:1254–61.
8. DiNicolantonio JJ, Mangan D, O'Keefe JH. Copper deficiency May be a leading cause of ischaemic heart disease. *Open Heart*. 2018;5:e000784.
9. Ejaz HW, Wang W, Lang M. (2020) Copper Toxicity Links to Pathogenesis of Alzheimer's Disease and Therapeutics Approaches. *Int J Mol Sci* 21.
10. Zhu SY, Zhou WQ, Niu YY, Zheng C, Liu X, Zhang YY, Yu C. COX17 restricts renal fibrosis development by maintaining mitochondrial copper homeostasis and restoring complex IV activity. *Acta Pharmacol Sin*. 2023;44:2091–102.
11. Shanhbagh VC, Gudekar N, Jasmer K, Papageorgiou C, Singh K, Petris MJ. Copper metabolism as a unique vulnerability in cancer. *Biochim Biophys Acta Mol Cell Res*. 2021;1868:118893.
12. Pavithra V, Sathisha TG, Kasturi K, Mallika DS, Amos SJ, Ragunatha S. Serum levels of metal ions in female patients with breast cancer. *J Clin Diagn Res*. 2015;9:BC25–c27.
13. Lener MR, Scott RJ, Wiechowska-Kozłowska A, Serrano-Fernandez P, Baszuk P, Jaworska-Bieniek K, Sukiennicki G, Marciniak W, Muszynska M, Kładny J, Gro-mowski T, Kaczmarek K, Jakubowska A, Lubinski J. Serum concentrations of selenium and copper in patients diagnosed with pancreatic Cancer. *Cancer Res Treat*. 2016;48:1056–64.
14. Guo J, Cheng J, Zheng N, Zhang X, Dai X, Zhang L, Hu C, Wu X, Jiang Q, Wu D, Okada H, Pandolfi PP, Wei W. Copper promotes tumorigenesis by activating the PDK1-AKT oncogenic pathway in a copper transporter 1 dependent manner. *Adv Sci (Weinh)*. 2021;8:e2004303.
15. Yan T, Yang H, Meng Y, Li H, Jiang Q, Liu J, Xu C, Xue Y, Xu J, Song Y, Chu X, Wang L, Chen X, Che F. Targeting copper death genotyping associated gene RARRES2 suppresses glioblastoma progression and macrophages infiltration. *Cancer Cell Int*. 2023;23:105.
16. Davis CI, Gu X, Kiefer RM, Ralle M, Gade TP, Brady DC. Altered copper homeostasis underlies sensitivity of hepatocellular carcinoma to copper chelation. *Metalomics*. 2020;12:1995–2008.
17. He F, Chang C, Liu B, Li Z, Li H, Cai N, Wang HH. (2019) Copper (II) Ions Activate Ligand-Independent Receptor Tyrosine Kinase (RTK) Signaling Pathway. *Biomed Res Int* 2019, 4158415.
18. Song G, Dong H, Ma D, Wang H, Ren X, Qu Y, Wu H, Zhu J, Song W, Meng Y, Wang L, Liu T, Shen X, Zhao Y, Zhu C. Tetrahedral framework nucleic acid delivered RNA therapeutics significantly attenuate pancreatic Cancer progression via Inhibition of CTR1-Dependent copper absorption. *ACS Appl Mater Interfaces*. 2021;13:46334–42.
19. Poursani EM, Mercatelli D, Raininga P, Bell JL, Saletta F, Kohane FV, Neumann DP, Zheng Y, Rouaen JRC, Jue TR, Michniewicz FT, Schadel P, Kasiou E, Tsoli M, Cirillo G, Waters S, Shai-Hee T, Cazzoli R, Brettelle M, Slapetova I, Kasherman M, Whan R, Souza-Fonseca-Guimaraes F, Vahdat L, Ziegler D, Lock JG, Giorgi FM, Khanna K, Vittorio O. Copper chelation suppresses epithelial-mesenchymal transition by Inhibition of canonical and non-canonical TGF-beta signaling pathways in cancer. *Cell Biosci*. 2023;13:132.
20. Vitaliti A, Roccatani I, Iorio E, Perta N, Gismondi A, Chirico M, Pisanu ME, Di Marino D, Canini A, De Luca A, Rossi L. AKT-driven epithelial-mesenchymal transition is affected by copper bioavailability in HER2 negative breast cancer cells via a LOXL2-independent mechanism. *Cell Oncol (Dordt)*. 2023;46:93–115.
21. Onuma T, Mizutani T, Fujita Y, Yamada S, Yoshida Y. Copper content in ascitic fluid is associated with angiogenesis and progression in ovarian cancer. *J Trace Elem Med Biol*. 2021;68:126865.
22. Semenza GL. HIF-1: using two hands to flip the angiogenic switch. *Cancer Metastasis Rev*. 2000;19:59–65.
23. Xie H, Kang YJ. Role of copper in angiogenesis and its medicinal implications. *Curr Med Chem*. 2009;16:1304–14.
24. Ning N, Shang Z, Liu Z, Xia Z, Li Y, Ren R, Wang H, Zhang Y. A novel microtubule inhibitor promotes tumor ferroptosis by attenuating SLC7A11/GPX4 signaling. *Cell Death Discovery*. 2023;9:453.
25. Vitaliti A, De Luca A, Rossi L. (2022) Copper-Dependent Kinases and Their Role in Cancer Inception, Progression and Metastasis. *Biomolecules* 12.
26. Liggett WH Jr., Sidransky D. Role of the p16 tumor suppressor gene in cancer. *J Clin Oncol*. 1998;16:1197–206.
27. Yi L, Kaler S. ATP7A trafficking and mechanisms underlying the distal motor neuropathy induced by mutations in ATP7A. *Ann N Y Acad Sci*. 2014;1314:49–54.
28. Jardim DL, Goodman A, de Melo Gagliato D, Kurzrock R. The challenges of tumor mutational burden as an immunotherapy biomarker. *Cancer Cell*. 2021;39:154–73.
29. Vitale I, Manic G, Coussens LM, Kroemer G, Galluzzi L. Macrophages and metabolism in the tumor microenvironment. *Cell Metab*. 2019;30:36–50.
30. Wang Y, Wang D, Yang L, Zhang Y. Metabolic reprogramming in the immunosuppression of tumor-associated macrophages. *Chin Med J (Engl)*. 2022;135:2405–16.
31. Taylor V, Suter U. Epithelial membrane protein-2 and epithelial membrane protein-3: two novel members of the peripheral Myelin protein 22 gene family. *Gene*. 1996;175:115–20.
32. Uhlen M, Fagerberg L, Hallstrom BM, Lindskog C, Oksvold P, Mardinoglu A, Sivertsson A, Kampf C, Sjostedt E, Asplund A, Olsson I, Edlund K, Lundberg E, Navani S, Sztybel CA, Odeberg J, Djureinovic D, Takanen JO, Hober S, Alm T, Edqvist PH, Berling H, Tegel H, Mulder J, Roberg J, Nilsson P, Schwenk JM, Hamsten M, von Feilitzen K, Forsberg M, Persson L, Johansson F, Zwaan M, von Heijne G, Nielsen J, Ponten F. Proteomics. Tissue-based map of the human proteome. *Science*. 2015;347:1260419.
33. Martija AA, Krauss A, Bachle N, Doth L, Christians A, Krunic D, Schneider M, Helm D, Will R, Hartmann C, Herold-Mende C, von Deimling A, Pusch S. EMP3 sustains oncogenic EGFR/CDK2 signaling by restricting receptor degradation in glioblastoma. *Acta Neuropathol Commun*. 2023;11:177.
34. Wei L, Li L, Liu L, Yu R, Li X, Luo Z. Knockdown of Annexin-A1 inhibits growth, migration and invasion of glioma cells by suppressing the PI3K/Akt signaling pathway. *ASN Neuro*. 2021;13:17590914211001218.
35. Wu Q, Yin X, Zhao W, Xu W, Chen L. Downregulation of SFRP2 facilitates cancer stemness and radioresistance of glioma cells via activating Wnt/beta-catenin signaling. *PLoS ONE*. 2021;16:e0260864.
36. Zhang L, Zhang P, Tan Y, Feng Q, Zhao R. MicroRNA-522-3p plays an oncogenic role in glioblastoma through activating Wnt/beta-catenin signaling pathway via targeting SFRP2. *NeuroReport*. 2021;32:88–98.
37. Thompson EM, Stoker AW. (2021) A review of DUSP26: structure, regulation and relevance in human disease. *Int J Mol Sci* 22.
38. Bourgonje AM, Verrijp K, Schepens JT, Navis AC, Piepers JA, Palmén CB, van den Eijnden M, van Hooft R, Wesseling P, Leenders WP, Hendriks WJ. Comprehensive protein tyrosine phosphatase mRNA profiling identifies new regulators in the progression of glioma. *Acta Neuropathol Commun*. 2016;4:96.
39. Guo G, Gong K, Ali S, Ali N, Shallwani S, Hatanpaa KJ, Pan E, Mickey B, Burma S, Wang DH, Kesari S, Sarkaria JN, Zhao D, Habib AA. A TNF-JNK-Axl-ERK signaling axis mediates primary resistance to EGFR inhibition in glioblastoma. *Nat Neurosci*. 2017;20:1074–84.
40. Zimu Z, Jia Z, Xian F, Rui M, Yuting R, Yuan W, Tianhong W, Mian M, Yinlong L, Erfang S. Decreased expression of PACSIN1 in brain glioma samples predicts poor prognosis. *Front Mol Biosci*. 2021;8:696072.
41. Cheng SX, Tu Y, Zhang S. FoxM1 promotes glioma cells progression by up-regulating Anxa1 expression. *PLoS ONE*. 2013;8:e72376.
42. Zhang X, Lv QL, Huang YT, Zhang LH, Zhou HH. Akt/FoxM1 signaling pathway-mediated upregulation of MYBL2 promotes progression of human glioma. *J Exp Clin Cancer Res*. 2017;36:105.
43. Wang J, Qin D, Tao Z, Wang B, Xie Y, Wang Y, Li B, Cao J, Qiao X, Zhong S, Hu X. Identification of cuproptosis-related subtypes, construction of a prognosis model, and tumor microenvironment landscape in gastric cancer. *Front Immunol*. 2022;13:1056932.
44. Reisländer T, Groelly FJ, Tarsounas M. DNA damage and Cancer immunotherapy: A STING in the Tale. *Mol Cell*. 2020;80:21–8.
45. Feng M, Jiang W, Kim BYS, Zhang CC, Fu YX, Weissman IL. Phagocytosis checkpoints as new targets for cancer immunotherapy. *Nat Rev Cancer*. 2019;19:568–86.
46. Li E, Qiao H, Sun J, Ma Q, Lin L, He Y, Li S, Mao X, Zhang X, Liao B. Cuproptosis-related gene expression is associated with immune infiltration and CD47/CD24 expression in glioblastoma, and a risk score based on these genes can predict the survival and prognosis of patients. *Front Oncol*. 2023;13:1011476.
47. Vo TTT, Peng TY, Nguyen TH, Bui TNH, Wang CS, Lee WJ, Chen YL, Wu YC, Lee IT. The crosstalk between copper-induced oxidative stress and Cuproptosis:

- a novel potential anticancer paradigm. *Cell Communication Signaling*: CCS. 2024;22:353.
48. Jin J, Ma M, Shi S, Wang J, Xiao P, Yu HF, Zhang C, Guo Q, Yu Z, Lou Z, Teng CB. Copper enhances genotoxic drug resistance via ATOX1 activated DNA damage repair. *Cancer Lett*. 2022;536:215651.
  49. Liu H. Pan-cancer profiles of the Cuproptosis gene set. *Am J cancer Res*. 2022;12:4074–81.
  50. Zhang G, Wang N, Ma S, Tao P, Cai H. Comprehensive analysis of the effects of the cuproptosis-associated gene SLC31A1 on patient prognosis and tumor microenvironment in human cancer. *Translational cancer Res*. 2024;13:714–37.
  51. Lutsenko S. (2021) Dynamic and cell-specific transport networks for intracellular copper ions. *J Cell Sci* 134.
  52. Denoyer D, Masaldan S, La Fontaine S, Cater MA. Targeting copper in cancer therapy: 'copper that cancer'. *Metalloomics*. 2015;7:1459–76.
  53. Xie J, Yang Y, Gao Y, He J. Cuproptosis: mechanisms and links with cancers. *Mol Cancer*. 2023;22:46.
  54. Cordero MD, Alcocer-Gomez E, Ryffel B. Gain of function mutation and inflammasome driven diseases in human and mouse models. *J Autoimmun*. 2018;91:13–22.
  55. Nagai M, Vo NH, Ogawa S, Chimmanamada L, Inoue D, Chu T, Beaudette-Zlatanova J, Lu BC, Blackman R, Barsoum RK, Koya J, K., and, Wada Y. The oncology drug elesclomol selectively transports copper to the mitochondria to induce oxidative stress in cancer cells. *Free Radic Biol Med*. 2012;52:2142–50.
  56. Ismail M, Yang W, Li Y, Wang Y, He W, Wang J, Muhammad P, Chaston TB, Rehman FU, Zheng M, Lovejoy DB, Shi B. Biomimetic Dp44mT-nanoparticles selectively induce apoptosis in Cu-loaded glioblastoma resulting in potent growth inhibition. *Biomaterials*. 2022;289:121760.
  57. Baldari S, Di Rocco G, Heffern MC, Su TA, Chang CJ, Toietta G. (2019) Effects of copper chelation on BRAF(V600E) positive Colon carcinoma cells. *Cancers (Basel)* 11.
  58. Li X, Li N, Huang L, Xu S, Zheng X, Hamsath A, Zhang M, Dai L, Zhang H, Wong JJ, Xian M, Yang CT, Liu J. (2020) Is Hydrogen Sulfide a Concern During Treatment of Lung Adenocarcinoma With Ammonium Tetrathiomolybdate? *Front Oncol* 10, 234.
  59. Belyaeva EA, Sokolova TV, Emelyanova LV, Zakharova IO. (2012) Mitochondrial electron transport chain in heavy metal-induced neurotoxicity: effects of cadmium, mercury, and copper. *TheScientificWorldJournal* 2012, 136063.
  60. Xue Q, Yan D, Chen X, Li X, Kang R, Klionsky DJ, Kroemer G, Chen X, Tang D, Liu J. Copper-dependent autophagic degradation of GPX4 drives ferroptosis. *Autophagy*. 2023;19:1982–96.
  61. Mi J, Luo J, Zeng H, Zhang H, Jamil M, Abdel-Maksoud MA, Zakri AM, Alfuraydi AA, Zhang N, Xiao M. Elucidating cuproptosis-related gene SLC31A1 diagnostic and prognostic values in cancer. *Am J Translational Res*. 2023;15:6026–41.
  62. Fu H, Dong S, Li K. Identification of SLC31A1 as a prognostic biomarker and a target for therapeutics in breast cancer. *Sci Rep*. 2024;14:25120.
  63. Xue R, Qin C, Li L, Huang L, Tang K, Chen J, Liang H, Xu H, Qin X, Yang C, Tan Q. SRF/SLC31A1 signaling promotes Cuproptosis induced by Celastrol in NSCLC. *Int Immunopharmacol*. 2025;148:114165.

### Publisher's note

Springer Nature remains neutral with regard to jurisdictional claims in published maps and institutional affiliations.